# Effective elastic properties of transversely isotropic materials with concave pores

K. Du, L. Cheng, Jean-François Barthélémy, I. Sevostianov, A. Giraud, A. Adessina

Version of Record: https://www.sciencedirect.com/science/article/pii/S0167663620306980
Manuscript_1e5588eff927c74dc13c132e1201a919

# Effective elastic properties of transversely isotropic materials with concave pores

K. Du[a], L. Cheng[a], J. F. Barthélémy[b], I. Sevostianov[c], A. Giraud[a,*], A. Adessina[b]

[a] *GeoRessources Laboratory, Université de Lorraine (ENSG), CNRS, CREGU, F-54518 Vandoeuvre-lès-Nancy, France*
[b] *Cerema, Project-team DIMA, 110 rue de Paris, BP 214, 77487 Provins Cedex, France*
[c] *Department of Mechanical and Aerospace Engineering, New Mexico State University, Las Cruces, NM 88001, USA*

**Abstract**

The aim of this paper is to extend recent works devoted to the study of the effect of 3*D* pores of concave shape embedded in isotropic matrix to the case of transversely isotropic (*TI*) matrix. In the first part of the paper, approximate relations for the compliance contribution tensor of pores of two reference shapes, supersphere and axisymmetrical superspheroid, are developed on the basis of 3*D* Finite Element Modelling, recently presented in a companion paper, and known exact solutions for the limiting cases of spherical pores and circular crack. In the second part application to effective elastic coefficients of transversely isotropic materials such as clay rocks, in the frame of homogenization theory is presented to illustrate the impact of concavity parameter on overall properties.

*Keywords:* concave shape, supersphere, superspheroid, compliance contribution tensor, effective elastic properties, transversely isotropic matrix

## 1. Introduction

In the present paper, we analyze the effect of the concavity of pores on the overall elastic properties of a porous material with transversely-isotropic solid phase. For this goal, we use two homogenization techniques: Mori-Tanaka-Benveniste scheme and Maxwell scheme. Both of them are based on the solution for a single inhomogeneity problem and can be easily formulated for ellipsoidal inhomogeneities using Eshelby results [1]. Non-ellipsoidal shapes of the inhomogeneities are not so well studied and most of the results are obtained in $2-D$ by conformal mapping [2]. For three-dimensional case, the problem of *irregular* (non-ellipsoidal) inhomogeneities reduces to integral equations and generally requires computational approaches although, in some cases, solution can be obtained in the form of infinite series, see, for example [3] . They can be generally subdivided onto two groups: (i) direct computation of stress and strain fields for a given (deterministic) microstructure by discretizing the domain and using the FEM, and then post-processing the averages of the stress and strain fields (see, for example, [4]) and (ii) computation of the contribution of one isolated inhomogeneity into the effective elastic properties as a function of its shape. The latter results constitute basic building blocks for theoretical models that cover diverse orientation distributions and concentrations of inhomogeneities.
[5] analyzed shape effects on the effective elastic and thermal properties of the composites containing randomly oriented and distributed spherical, octahedral, cubical and tetrahedral particles. [6] proposed to evaluate effect of pores of irregular shape on the overall elastic moduli using pore projected areas. This approach works well for prediction of the overall Young's moduli in different directions. [7] performed comprehensive numerical analysis of the pore shape on the overall properties of solids with porosity levels up to 25%. [8] compared predictions of overall elastic properties of composites reinforced with particles of a different polyhedral shapes by FEM and micromechanical schemes. The results of the two approaches are in good agreement for volume fractions up to 30% for all studied material combinations. The inverse problem – design of material microstructure has been has been done by Zohdi [9], who determine optimal geometrical and mechanical properties of inhomogeneities for prescribed overall elastic

*Corresponding author
*Email address:* albert.giraud@univ-lorraine.fr (A. Giraud )

moduli.
Effect of the concavity factor of superspheres and axisymmetric concave pores was analyzed in the works of [10, 11, 12]. The authors supplemented finite element modelling with analytical approximations for compliance contribution tensors of pores of such shapes. These results were used to calculate overall elastic properties of materials with multiple concave pores: oolitic rock [13] and $3-D$ printed $Si_3N_4$ ceramics [14]. All the mentioned results have been obtained for materials with isotropic matrix. The number of explicit results on elastic properties of heterogeneous materials with anisotropic matrix is substantially smaller. Piezoelectric properties of transversely isotropic materials containing circular fibers aligned with the axes of symmetry of the matrix have been calculated using various homogenization techniques by [15]. [16] calculated compliance contribution tensor for a spheroidal inhomogeneity of arbitrary aspect ratio embedded in a transversely-isotropic material. [17] calculated effective elastodynamic properties of transversely isotropic rocks containing aligned spherical and strongly oblate spheroidal pores. Effective porothermoelastic properties of transversely isotropic rocks such as mudstones, argillites, shales have been studied in the frame of Effective Media Theory (*EMT*), by [18]. [19] calculated overall properties of transversely-isotropic clay containing spherical inhomogeneities. [20] calculated overall properties of a transversely-isotropic material containing parallel circular cracks. [21] used approach developed by [22] to calculate overall properties of a transversely-isotropic material containing arbitrarily oriented cracks. This result was used by [23] to estimate properties of a transversely-isotropic material with multiple arbitrarily oriented oblate inhomogeneities and applied to calculation of the overall properties of dentin.
In the text to follow, we use the recent numerical results of [24] where compliance contribution tensors of concave pores in a transversely-isotropic material are obtained. We suggest an analytical approximation of the components of these tensor using approach of [25] and evaluate overall elastic properties of transversely-isotropic materials containing such pores. The results are illustrated by example of shale rock containing concave pores.

## 2. Compliance contribution tensor of a concave pore

Refer to appendices 7 and 8 for background on tensors and property contribution tensors. Recently [24] calculated components of the compliance contribution tensors of superspheroidal and axisymmetric superspheroidal pores embedded in a transversely-isotropic material numerically.

- superspheroidal pore

$$|\frac{x_1}{a}|^{2p}+|\frac{x_2}{a}|^{2p}+|\frac{x_3}{\varsigma a}|^{2p}=1 \tag{1}$$

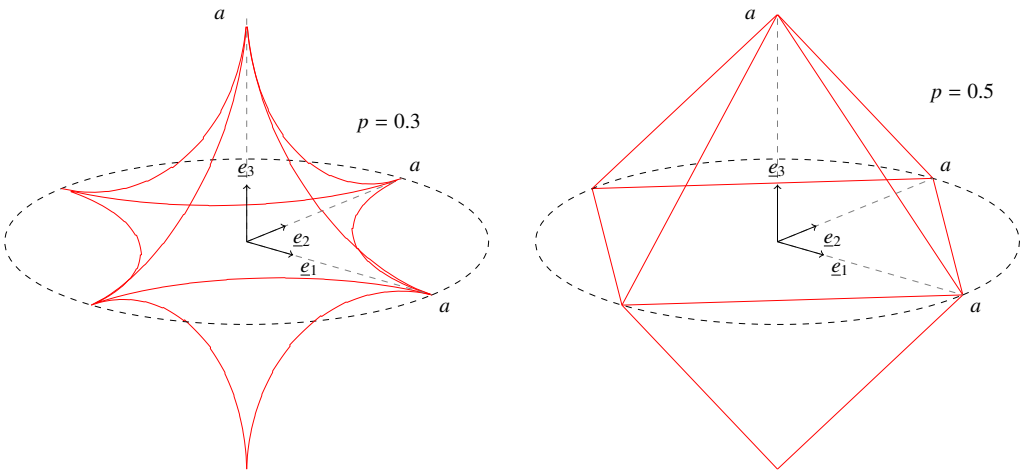


Figure 1: Superspherical pore (relation (1) with $\varsigma = 1$)

- axisymmetrical superspheroidal pore

$$\left(\frac{x_1^2+x_2^2}{a^2}\right)^p + \left|\frac{x_3}{\varsigma a}\right|^{2p} = 1 \tag{2}$$

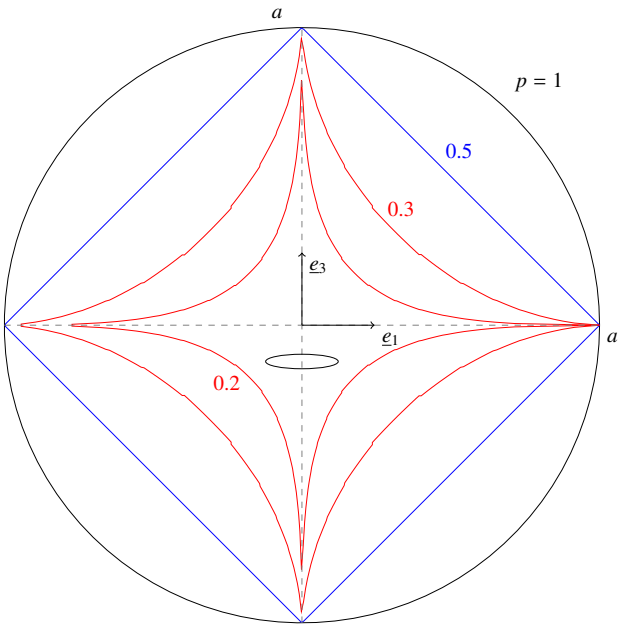


Figure 2: $2D$ representation in diametral plane of a $3D$ axisymmetrical superspheroidal pore, with $\varsigma = 1$ and symmetry axis $x_3$

$p$, $\varsigma$ and $a$ respectively denote non dimensional concavity parameter, non dimensional aspect ratio and semi-lengths in plane $Ox_1x_2$ (dimension of length $[a] = L$). Theses shapes are convex in the range $p > 0.5$ and concave for $0 < p < 0.5$. Both shapes degenerate into a spheroid is with $p = 1$. In what follows we will only consider $\varsigma = 1$, the first shape is then a supersphere, and the second shape obtained by a rotation about symmetry axis $x_3$. Supersphere and axisymmetrical superspheroid coincide with sphere in the case $p = 1$ but strongly differ in the limiting case $p \to 0$: supersphere tends to three orthogonal needles along coordinates axes and superspheroid tends to a circular crack of unit radius crossed by a perpendicular needle along symmetry axis $x_3$.
Compliance contribution tensor $\mathbb{H}_0^{\mathcal{E}}$ of a superspherical pore aligned with the direction of a $TI$ matrix, with symmetry axis $x_3$, respects tetragonal symmetry. With three orthogonal planes of symmetry (with normal $\underline{e}_i$) and equivalence between $x_1$ and $x_2$ axes, its 6 independent elastic coefficients are $H^{\mathcal{E}}_{1111}$, $H^{\mathcal{E}}_{1122}$, $H^{\mathcal{E}}_{1133}$, $H^{\mathcal{E}}_{3333}$, $H^{\mathcal{E}}_{2323}$, $H^{\mathcal{E}}_{1212}$. Compliance contribution tensor of an axisymmetric superspherspheroidal pore aligned with the $TI$ matrix is transversely isotropic with 5 independent elastic coefficients, $H^{\mathcal{E}}_{1111}$, $H^{\mathcal{E}}_{1122}$, $H^{\mathcal{E}}_{1133}$, $H^{\mathcal{E}}_{3333}$, $H^{\mathcal{E}}_{2323}$. $\mathbb{H}_0^{\mathcal{E}}$ can be written in terms of the transversely isotropic tensor basis $\mathbb{E}$ detailed in appendix (8) as

$$\mathbb{H}_0^{\mathcal{E}} = \sum_{i=1}^{6} h_i \, \mathbb{E}_i \tag{3}$$

Average compliance contribution tensors $\mathbb{H}_0^{\mathcal{E}}$ of superspherical and axisymmetrical superspheroidal pores have been numerically calculated by using $3D$ Finite Element Method ($FEM$), see [24] considering $TI$ matrix with elastic properties of a shale (see Tables 1-2).

Table 1: Reference transversely isotropic elastic parameters

| $E_1^0$ (GPa) | $E_3^0$ (GPa) | $\nu_{12}^0$ | $\nu_{31}^0$ | $G_{31}^0$ (GPa) |
|---|---|---|---|---|
| 20.44 | 11.306 | 0.1027 | 0.1798 | 1.5851 |

Table 2: Reference transversely isotropic elastic parameters: $C_{ijkl}^0$ components of $\mathbb{C}_0$ tensor and related $c_i$ components in transversely isotropic tensor basis $\mathbb{E}_i$

| $C_{1111}^0$ (GPa) | $C_{3333}^0$ (GPa) | $C_{1122}^0$ (GPa) | $C_{1133}^0$ (GPa) | $C_{2323}^0$ (GPa) |
|---|---|---|---|---|
| 22.3639 | 12.9994 | 3.8275 | 4.7092 | 1.5851 |
| $c_1$ (GPa) | $c_3$ (GPa) | $c_3 = c_4$ (GPa) | $c_5$ (GPa) | $c_6$ (GPa) |
| 12.9994 | 26.1914 | 6.65983 | 18.5363 | 3.1702 |

Numerical results of [24] are summarized in Tables (7-8) (see appendix 9). In the particular case of an ellipsoidal pore $\mathcal{E}$ embedded in an infinite matrix 0 of stiffness $\mathbb{C}_0$ and compliance $\mathbb{S}_0$ tensors, compliance $\mathbb{H}_0^{\mathcal{E}}$ and stiffness $\mathbb{N}_0^{\mathcal{E}}$ contribution tensors are analytical and write (see [26] for details) :

$$\mathbb{H}_0^{\mathcal{E}} = \left[(\mathbb{S}_{\mathcal{E}} - \mathbb{S}_0)^{-1} + \mathbb{Q}_0^{\mathcal{E}}\right]^{-1}, \quad \mathbb{N}_0^{\mathcal{E}} = \left[(\mathbb{C}_{\mathcal{E}} - \mathbb{C}_0)^{-1} + \mathbb{P}_0^{\mathcal{E}}\right]^{-1} \tag{4}$$

where $\mathbb{P}_0^{\mathcal{E}}$ and $\mathbb{Q}_0^{\mathcal{E}}$ denote the fourth order Hill's tensors [27] of the inhomogeneity, related by relation

$$\mathbb{Q}_0^{\mathcal{E}} = \mathbb{C}_0 : \left(\mathbb{I} - \mathbb{P}_0^{\mathcal{E}} : \mathbb{C}_0\right) \tag{5}$$

Strain Hill tensor $\mathbb{P}_0^{\mathcal{E}}$ of a spheroidal inhomogeneity aligned in a *TI* matrix may be found in [16, 28] and it is recalled for convenience in appendix 8. In the next Section we approximate these results analytically and then use them to calculate overall elastic properties of transversely isotropic matrix containing multiple concave pores.

## 3. Approximation formula for compliance contribution tensor of a superspherical or axisymmetrical superspheroidal pore embedded in a transversely isotropic host matrix

We investigate in this section the extension to transverse isotropy of approximation formula for the compliance contribution tensor of $3D$ pores of particular shapes previously presented. We restrict the study to the following assumptions

- same directions of symmetry between matrix and pore inclusion (*aligned* case)
- study is focused on the concavity parameter $p$
- in the case of superspherical pore, compliance contribution tensor respects tetragonal symmetry (6 independent components) but we will consider for applications random orientation distributions in the isotropic plane $x_1 - x_2$ ($x_3$ denotes the symmetry axis) on the one hand, in $3D$ space on the other hand. Related compliance contribution tensors respects transversely isotropic symmetry.

*3.1. Volume and surface area of superspherical and axisymmetrical superspheroidal pores*

Approximation formula may be obtained by using basic geometric information related to the considered reference shapes, supersphere and axisymmetrical superspheroid, defined in relations (1-2), with aspect ratio $\varsigma = 1$. These informations are volume, total surface area and projected areas onto planes $0x_ix_3$ (with $i = 1, 2$).. and corresponding volumes write ($\Gamma$ denotes Euler *Gamma* function, see [10, 12, 25] for details)

$$V^{\mathrm{se}}(p) = \frac{2}{3}\frac{\left(\Gamma\left[\frac{1}{2p}\right]\right)^3}{p^2\,\Gamma\left[\frac{3}{2p}\right]}, \quad V^{\mathrm{so}}(p) = \frac{4\pi}{3}\frac{\Gamma\left(\frac{1+2p}{2p}\right)\Gamma\left(\frac{1}{p}\right)}{\Gamma\left(\frac{3}{2p}\right)} \tag{6}$$

where superscripts se and so respectively refer to supersphere and axisymmetric superspheroid. In the range $0 < p \leq 1$, supersphere and axisymmetrical superspheroid with unit semi-length $a$ are superscribed by unit sphere of volume $V_0 = 4\pi/3$. Ratios $V^{\mathrm{se}}(p)/V_0$, $V^{\mathrm{so}}(p)/V_0$ and $V^{\mathrm{se}}(p)/V^{\mathrm{so}}(p)$ are presented in figure (3).. Supersphere and axisymmetrical superspheroid coincide with sphere in the case $p = 1$ but strongly differ in the limiting case $p \to 0$: supersphere tends to three orthogonal needles along coordinates axes and superspheroid tends to a circular crack of unit radius crossed by a perpendicular needle along symmetry axis $x_3$. . Except for some particular values of concavity parameter ($p = \frac{1}{4}, \frac{1}{2}, 1$), the total surface area needs to be calculated by numerical integration. As in [25], we use the surface area of the supersphere $A^{\mathrm{se}}(p)$ given by [29], and the surface area $A^{\mathrm{so}}(p)$ of the axisymmetrical superspheroid is given by the single integral accounting for symmetry of revolution

$$A^{\mathrm{so}}(p) = \int_0^1 \left(1 - x^{2p}\right)^{\frac{1}{2p}} \left(1 + x^{-2(1+2p)}\left(1 - x^{2p}\right)^{\frac{1-2p}{p}}\right)^{\frac{1}{2}} dx \tag{7}$$

The projection area $S_{\mathrm{proj}}(p)$ of both $3D$ shapes onto planes $x_ix_3$ ($i = 1, 2$, $x_3$ denotes symmetry axis of the axisymmetrical superspheroid) writes (Beta denotes Euler Beta function)

$$S_{\mathrm{proj}}(p) = \frac{2}{p}\mathrm{Beta}\left(1 + \frac{1}{2p}, \frac{1}{2p}\right) \tag{8}$$

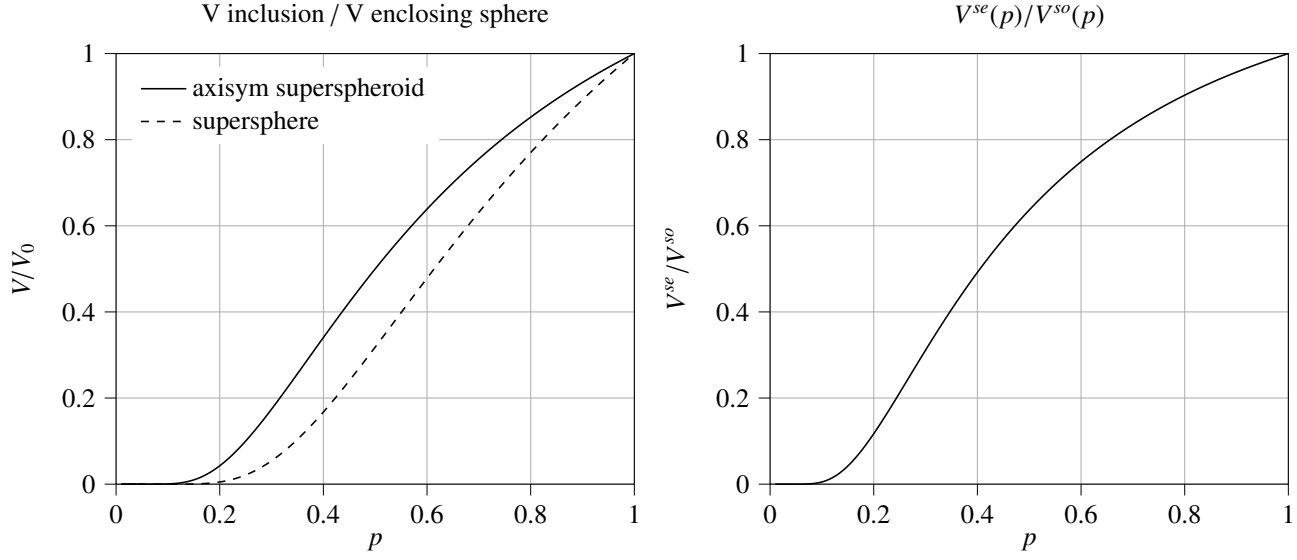


Figure 3: Left: ratios $V^{\mathrm{se}}(p)/V_0$ and $V^{\mathrm{so}}(p)/V_0$ functions of concavity parameter $p$, right: ratio $V^{\mathrm{se}}(p)/V^{\mathrm{so}}(p)$

*3.2. Approximation formula for superspherical pore*

We restrict this study to the range $0.2 \leq p \leq 1$, on the basis of [25] we propose approximation formula

$$H_{ijkl}(p) = \begin{cases} \dfrac{S_{\text{proj}}(p)/(V^{\text{se}}(p))^{2/3}}{S^{\text{octa}}_{\text{proj}}/\left(V^{\text{se}}_{\text{octa}}\right)^{2/3}}\ f^{\text{se-a}}_{ijkl}(p)\ H^{\text{octa}}_{ijkl} & 0.2 \leq p < 0.5 \quad \text{, no sum over } i \text{ and } j \\ \dfrac{A^{\text{se}}(p)/(V^{\text{se}}(p))^{2/3}}{A^{\text{octa}}_{\text{se}}/\left(V^{\text{se}}_{\text{octa}}\right)^{2/3}}\ f^{\text{se-b}}_{ijkl}(p)\ H^{\text{octa}}_{ijkl} & 0.5 \leq p \leq 1 \quad \text{, no sum over } i \text{ and } j \end{cases} \tag{9}$$

where *octa* denotes *octahedron* (particular case of supersphere at $p = 0.5$ represents an octahedron). Functions $f^{\text{se-a}}_{ijkl}(p)$ and $f^{\text{se-b}}_{ijkl}(p)$ are given in appendix. A quadratic fit has been considered for components $H_{iijj}$ (no sum over $i$ and $j$) whereas a fourth degree polynomial has been necessary to fit shear components $H_{1212}$, $H_{2323}$ . Comparisons between approximate relations (9) and finite element results are presented in figure 4. Maximal relative errors of approximate relations (9) compared to FEM results are given in table 3, they are lower than 4.%.

| $H^{\mathcal{E}}_{1111}$ | $H^{\mathcal{E}}_{1122}$ | $H^{\mathcal{E}}_{1133}$ | $H^{\mathcal{E}}_{3333}$ | $H^{\mathcal{E}}_{1212}$ | $H^{\mathcal{E}}_{1313}$ |
|---|---|---|---|---|---|
| 0.0349 | 0.03677 | 0.0350 | 0.0356 | 0.0061 | 0.0060 |

Table 3: Maximal relative errors of approximate relations compared to FEM results, $\left\| (H^{FEM}_{ijkl} - H^{FEM}_{ijkl})/H^{FEM}_{ijkl} \right\|_\infty$ for the superspherical pore with $p \in [0.2, 1]$

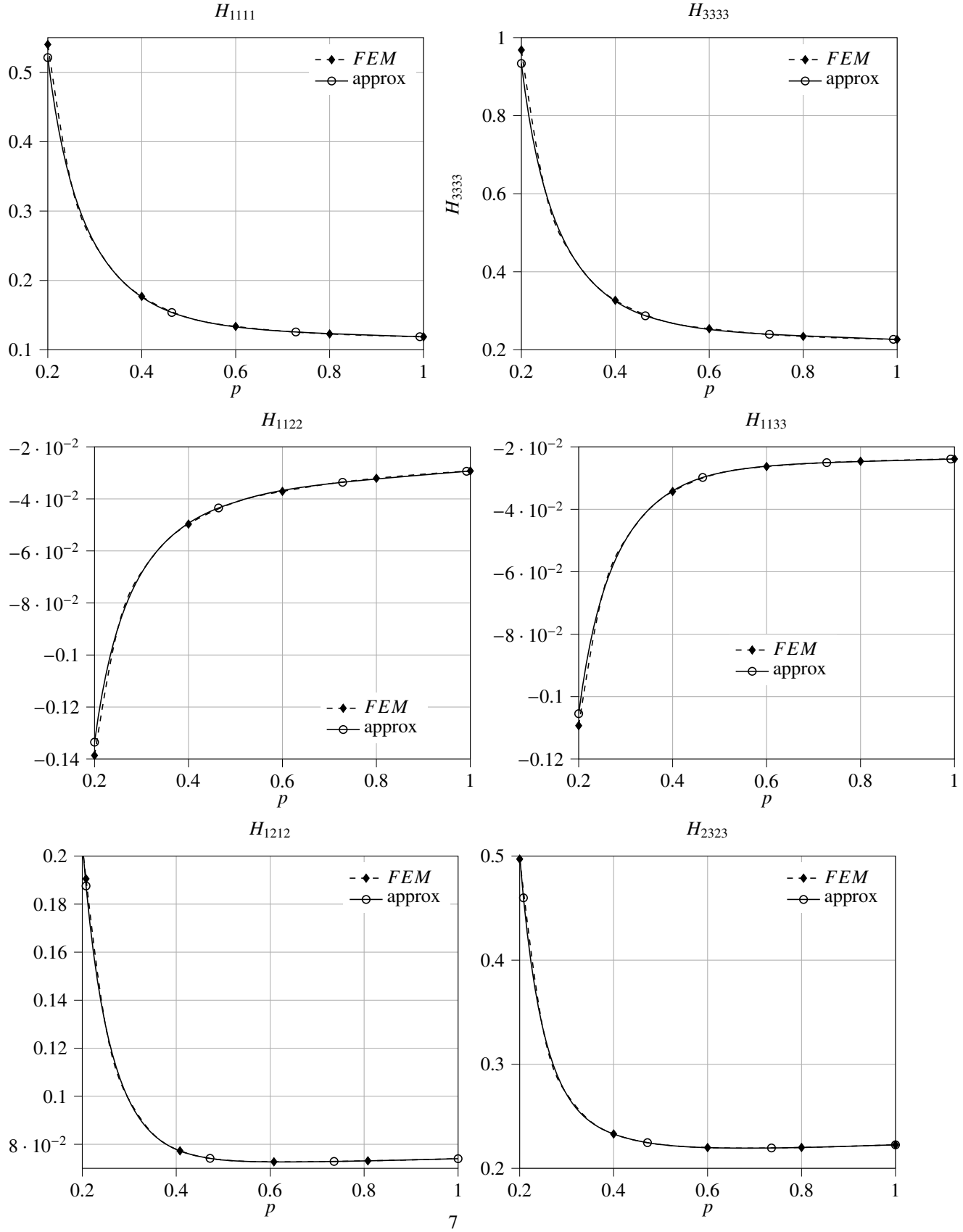


Figure 4: The 6 independent components $H_{ijkl}$ of the tetragonal compliance contribution tensor of a superspherical pore embedded in *TI* matrix, as a function of concavity parameter $p$. Comparison between *FEM* results (dashed lines) and approximate relations (plain lines).

*3.3. Approximation formula for axisymmetrical superspheroidal pore*

Similar approximation formula are proposed for components $H_{1111}$, $H_{1122}$, $H_{1133}$ but total surface area has been used instead of projection area, in the concave range $p < 0.5$.

$$H_{11ii}(p) = \begin{cases} \frac{A^{\text{so}}(p)/(V^{\text{so}}(p))^{2/3}}{A^{\text{octa}}_{\text{so}}/\left(V^{\text{so}}_{\text{octa}}\right)^{2/3}} \; f^{\text{so-a}}_{11ii}(p) \; H^{\text{octa}}_{11ii} & 0.2 \leq p < 0.5 \quad \text{, no sum over } i,\, i \in [1,2,3] \\ \frac{A^{\text{so}}(p)/(V^{\text{so}}(p))^{2/3}}{A^{\text{octa}}_{\text{so}}/\left(V^{\text{so}}_{\text{octa}}\right)^{2/3}} \; f^{\text{so-b}}_{11ii}(p) \; H^{\text{octa}}_{11ii} & 0.5 \leq p \leq 1 \quad \text{, no sum over } i,\, i \in [1,2,3] \end{cases} \tag{10}$$

where *octa* corresponds to the case ($p = 0.5$) which is not an *octahedron* but a double-conical shape. Functions $f^{\text{so-a}}_{11ii}(p)$ and $f^{\text{so-b}}_{11ii}(p)$ are given in appendix. Polynomials of degree 4 have been considered for both concave and convex domains in the range $0.2 < p < 1$. It may be noticed that semi-analytical approximations using the limiting cases of aligned circular crack $p \to 0$ and sphere $p \to 1$ may be used for components $H_{3333}$ and $H_{2323}$ (with $x_3$ symmetry axis of axisymmetrical superspheroid and *TI* matrix ). Approximate solutions writes

$$H_{3333}(p) = \frac{V^{\text{sphere}}}{V^{\text{so}}(p)} \left( \frac{1-p}{1-\alpha_o} H^c_{3333} + \frac{p-\alpha_o}{1-\alpha_o} H^{\text{sphere}}_{3333} \right), \quad \alpha_o = 0.19, \quad 0.2 \leq p \leq 1 \tag{11}$$

$$H_{2323}(p) = \begin{cases} f_{2323}(p) & 0.2 \leq p < 0.5 \\ H^{\text{sphere}}_{2323} & 0.5 \leq p \leq 1 \end{cases} \tag{12}$$

$$f_{2323}(p) = A + B \exp\left(-\omega(p - p_0)\right), \quad p_0 = 0.2 \tag{13}$$

Constants $A$ and $B$ are determined by using analytical solutions for the limiting cases of circular crack and sphere, which are imposed at $p = 0.2$ and $p = 0.5$ (difference between solutions of *axisymmetrical octahedron* $p = 0.5$ and sphere are not significant for $H_{2323}$ component).

$$f_{2323}(p = 0.2) = H^c_{2323} \frac{V^{\text{sphere}}}{V^{\text{so}}(0.2)}, \quad f_{2323}(p = 0.5) = H^{\text{sphere}}_{2323} \tag{14}$$

and then

$$A + B = H^c_{2323} \frac{V^{\text{sphere}}}{V^{\text{so}}(0.2)}, \quad A + B \exp\left(-0.3\,\omega\right) = H^{\text{sphere}}_{2323} \tag{15}$$

Constant $\omega$ is determined by fit of finite element results (see appendix 9 and [24] for details on finite element modellings). One obtains

$$A = 0.221795, \quad B = 0.591786, \quad \omega = 22 \tag{16}$$

Analytical solution for the compliance contribution tensor of a spheroidal pore aligned with the directions of a *TI* matrix is recalled in appendix. It may be noticed that approximation (11) for $H_{3333}$ component numerically coincides with the corresponding component of a spheroidal pore with same volume than superspheroidal pore :

$$H_{3333}(p) \approx H^{\text{spheroid}}_{3333}(\gamma(p)), \quad 0.2 \leq p \leq 1 \tag{17}$$

with

$$\gamma(p) = \frac{V^{\text{so}}(p)}{V^{\text{sphere}}} = \frac{\Gamma\left(\frac{1+2p}{2p}\right)\Gamma\left(\frac{1}{p}\right)}{\Gamma\left(\frac{3}{2p}\right)} \tag{18}$$

The analytical solution for the aligned spheroidal pore $H^{\text{spheroid}}_{ijkl}$ (it includes the particular case of the sphere, $H^{\text{sphere}}_{ijkl}$ with $\gamma(p = 1) = 1$) is deduced from the exact Hill tensor recalled in appendix 8. Comparisons between approximate

relations (10-11-12-17) and finite element results are presented in figure 5. Compliance contribution tensor of aligned axisymmetrical superspheroidal and spheroidal pores of same volume have quasi the same normal component $H_{3333}$. In other words, only the volume characterizes this component, not affected by concavity (superspheroid) of convexity (spheroid). It must be emphasized that it is not the case for all the other components $H_{ijkl}$, including the shear component $H_{2323}$, for which the concavity parameter $p$ is of major importance (volume is not sufficient to characterize compliance contribution tensor). Shear component $H_{1212}$ in the plane of transverse isotropy has been used to check accuracy of the symmetry of revolution by comparing to $H_{1111} - H_{1122})/2$. (see figure 6), it may be noticed that both coincide as expected.

Maximal relative errors of approximate relations (10-12-17) compared to FEM results are given in table 4, they are lower than 5.%.

| $H^{\mathcal{E}}_{1111}$ | $H^{\mathcal{E}}_{1122}$ | $H^{\mathcal{E}}_{1133}$ | $H^{\mathcal{E}}_{3333}$ | $H^{\mathcal{E}}_{1313}$ |
|---|---|---|---|---|
| 0.00133 | 0.00174 | 0.00297 | 0.04890 | 0.03425 |

Table 4: Maximal relative errors of approximate relations compared to FEM results, $\left\|(H^{FEM}_{ijkl} - H^{FEM}_{ijkl})/H^{FEM}_{ijkl}\right\|_{\infty}$ for the axisymetrical superspheroidal pore with $p \in [0.2, 1]$

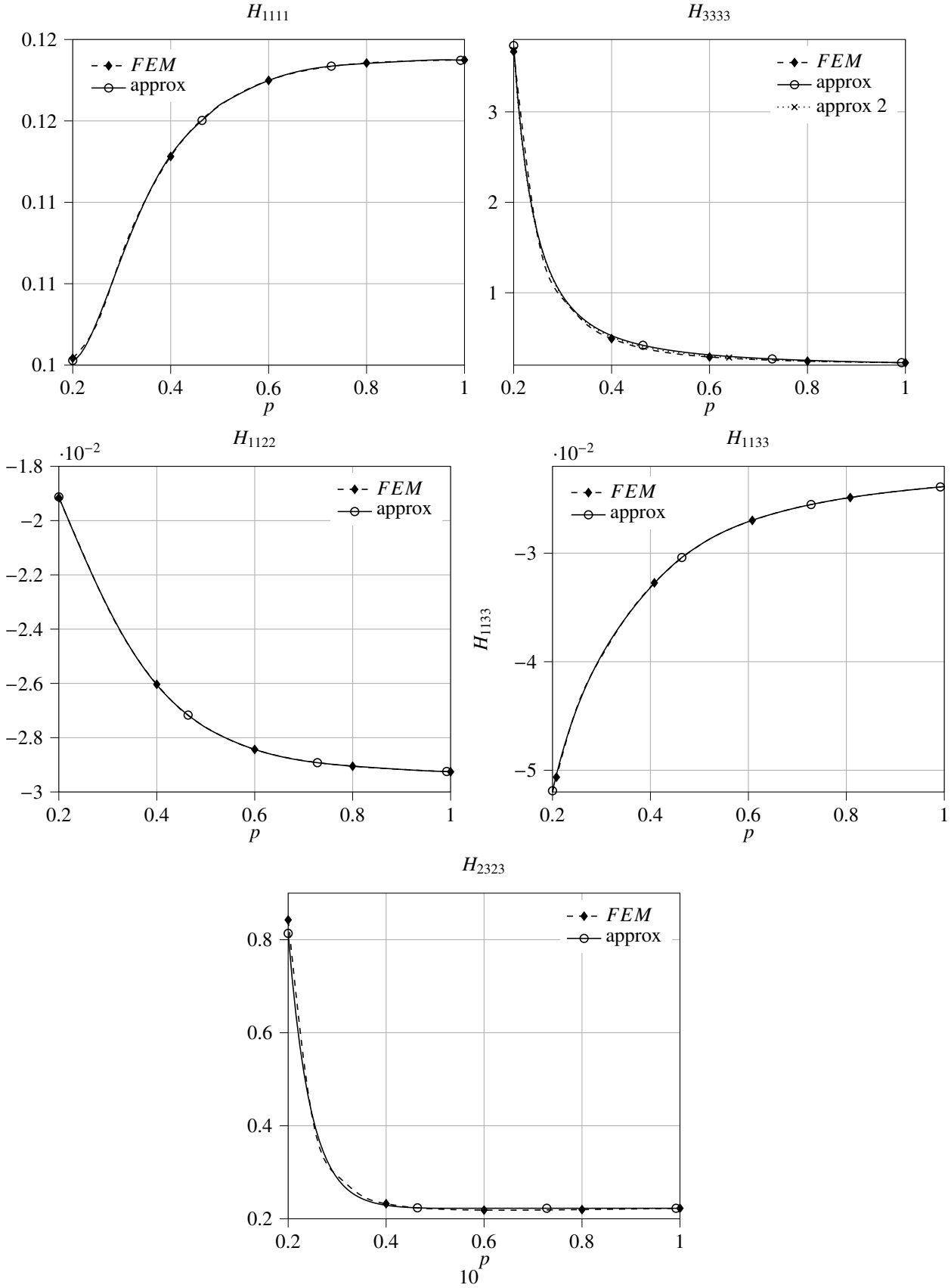


Figure 5: The 5 independent components $H_{ijkl}$ of the *TI* compliance contribution tensor of an axisymmetric superspheroidal pore embedded in *TI* matrix, as a function of concavity parameter $p$. Comparison between *FEM* results (dashed lines) and approximate relations (plain lines). Note that $H_{1212}$ is used to check accuracy of transverse isotropy by comparing to $(H_{1111} - H_{1122})/2$..

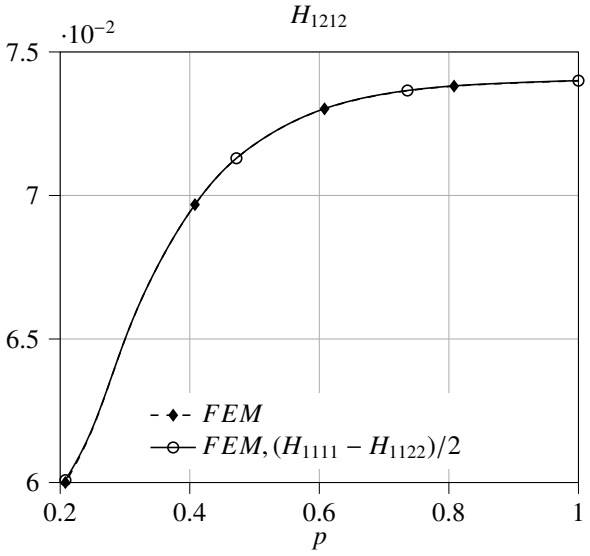


Figure 6: $H_{1212}$ component of the $TI$ compliance contribution tensor of an axisymmetric superspheroidal pore embedded in $TI$ matrix, as a function of concavity parameter $p$. $H_{1212}$ is used to check accuracy of transverse isotropy by comparing to $(H_{1111} - H_{1122})/2$..

## 4. Evaluation of the effective elastic properties of materials with transversely isotropic matrices

In this section, we calculate effective elastic properties using three homogenization techniques: Non Interaction Approximation, Mori Tanaka-Benveniste and Maxwell schemes (respectively referred with superscripts *NIA*, *MTB* and *MX*), see [30, 31, 26])

$$\mathbb{S}^{\text{NIA}} = \mathbb{S}_0 + \varphi \mathbb{H}_0^{\mathcal{E}}, \quad \mathbb{S}^{\text{MTB}} = \mathbb{S}_0 + \frac{\varphi}{1-\varphi}\mathbb{H}_0^{\mathcal{E}}, \quad \mathbb{S}^{\text{MX}} = \mathbb{S}_0 + \left[\frac{1}{\varphi}\left[\mathbb{H}_0^{\mathcal{E}}\right]^{-1} - \mathbb{Q}_0^{\Omega}\right]^{-1} \tag{19}$$

where $\varphi$ denotes the porosity. $\mathbb{Q}_0^{\Omega}$ denotes the second Hill tensor of the effective inclusion of the Maxwell scheme, which is supposed of spheroidal shape (with aspect ratio $\gamma^{\Omega}$) and aligned with the directions of the $TI$ host matrix. $\mathbb{Q}_0^{\Omega}$ is related to the strain Hill tensor $\mathbb{P}_0^{\Omega}$ by the relation (see appendix 8 for details):

$$\mathbb{Q}_0^{\Omega} = \mathbb{C}_0 : \left(\mathbb{I} - \mathbb{P}_0^{\Omega} : \mathbb{C}_0\right) \tag{20}$$

For numerical examples, we use elastic constants of shale and mudstone given in Tables 1 and 2 ([32, 19]. In what follows, effective elastic properties of porous clay matrix at mesoscopic scale are estimated by homogenizing micropores. We do not consider solid mineral inclusions of calcite and quartz which would need to be added for the transition from mesoscopic to the macroscopic scale (the centimeter scale of standard geomechanical laboratory tests).
The porosity of clay matrix $\varphi$ (denoted $f_p^I$ in [32]) is comprised in the range $\varphi \leq 0.30$ which has been considered for the sensitivity study.. It must be emphasized that most of the existing homogenization results do not account for anisotropy of the host matrix attributing the overall anisotropy to the microstructure of the pore space. This assumption is invalid for shale rock, in particular.
For geomaterials, the superspherical shape of pores is more realistic than the axisymmetric one since it approximately represents intergranular pores. We consider only a random orientation distribution of superspherical pores which does not violate the orientation of the symmetry axes of the transversely isotropic matrix. Transverse isotropic projection of compliance contribution tensor $\Pi^{TI}\left(\mathbb{H}_0^{\mathcal{E}}\right)$ will be used instead of the compliance contribution of the superspherical pore $\mathbb{H}_0^{\mathcal{E}}$. See appendix for detail, only components $H_{1111}$, $H_{1122}$ and $H_{1212}$ are modified, other components are equal, $H^{TI}_{1133} = H_{1133}$, $H^{TI}_{3333} = H_{3333}$, $H^{TI}_{2323} = H_{2323}$ ($H^{TI}_{ijkl}$ denotes $\left[\Pi^{TI}\left(\mathbb{H}_0^{\mathcal{E}}\right)\right]_{ijkl}$)

$$H^{TI}_{1111} = \frac{3\,H_{1111} + H_{1122} + 2\,H_{1212}}{4}, \quad H^{TI}_{1122} = \frac{H_{1111} + 3\,H_{1122} - 2\,H_{1212}}{4} \tag{21}$$

$$H^{TI}_{1212} = \frac{H_{1111} - H_{1122} + 2\,H_{1212}}{4} \tag{22}$$

Figure (7) illustrates the numerical difference between the tetragonal tensor $\mathbb{H}^{\mathcal{E}}_0$ and its *TI* projection $\Pi^{TI}\left(\mathbb{H}^{\mathcal{E}}_0\right)$.

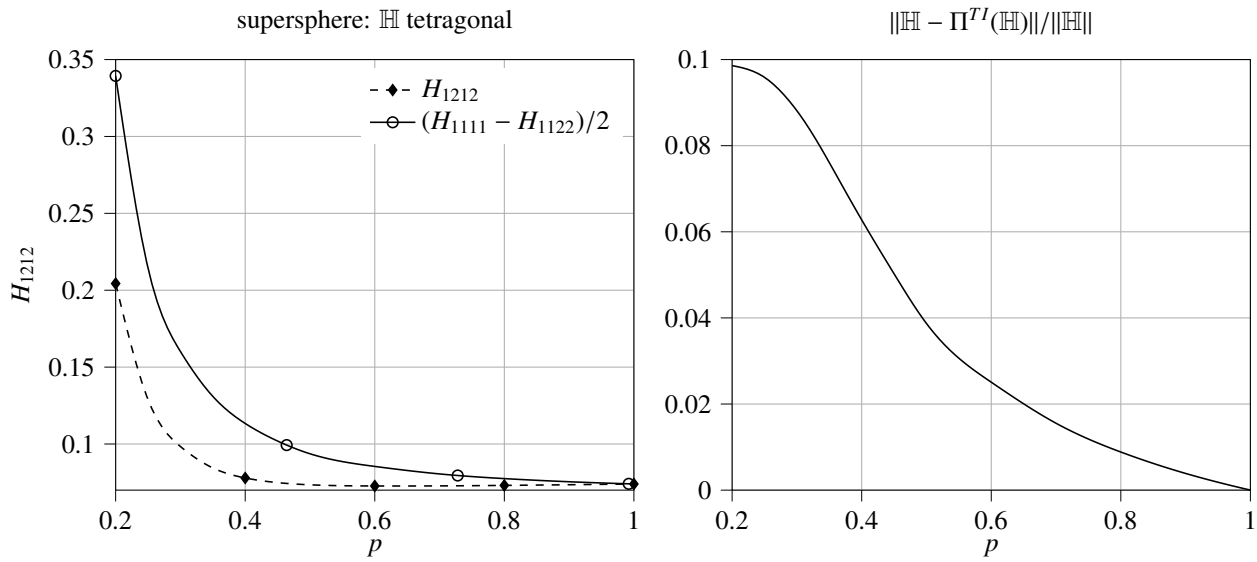


Figure 7: Left figure: comparison between $H_{1212}$ component and $(H_{1111} - H_{1122})/2$ to illustrate tetragonal symmetry of $\mathbb{H}$ tensor. Right figure: relative distance between $\mathbb{H}$ tensor and its *TI* projection as a function of concavity parameter. This relative distance is equal to zero in the case of the spherical inclusion $p = 1$.

### *4.1. Aligned axisymmetric superspheroidal pores*

Effective elastic coefficients $E_1^{\mathrm{MTB}}$ , $E_3^{\mathrm{MTB}}$ , $G_{31}^{\mathrm{MTB}}$ obtained with Mori-Tanaka-Benveniste (*MTB*) approximation are presented in figure (8). Approximation formula (10-11-12) deduced from *FEM* are compared to approximation of compliance contribution tensor of an oblate spheroidal pore of same volume (semi axis length of axisymmetrical superspheroid is equal to the greater semi axis length of the oblate spheroid) ):

$$H_{ijkl}(p) \approx H^{\mathrm{spheroid}}_{ijkl}(\gamma(p)), \quad 0.2 \leq p \leq 1 \tag{23}$$

with aspect ratio of oblate spheroid $\gamma(p)$ defined by relation (18)

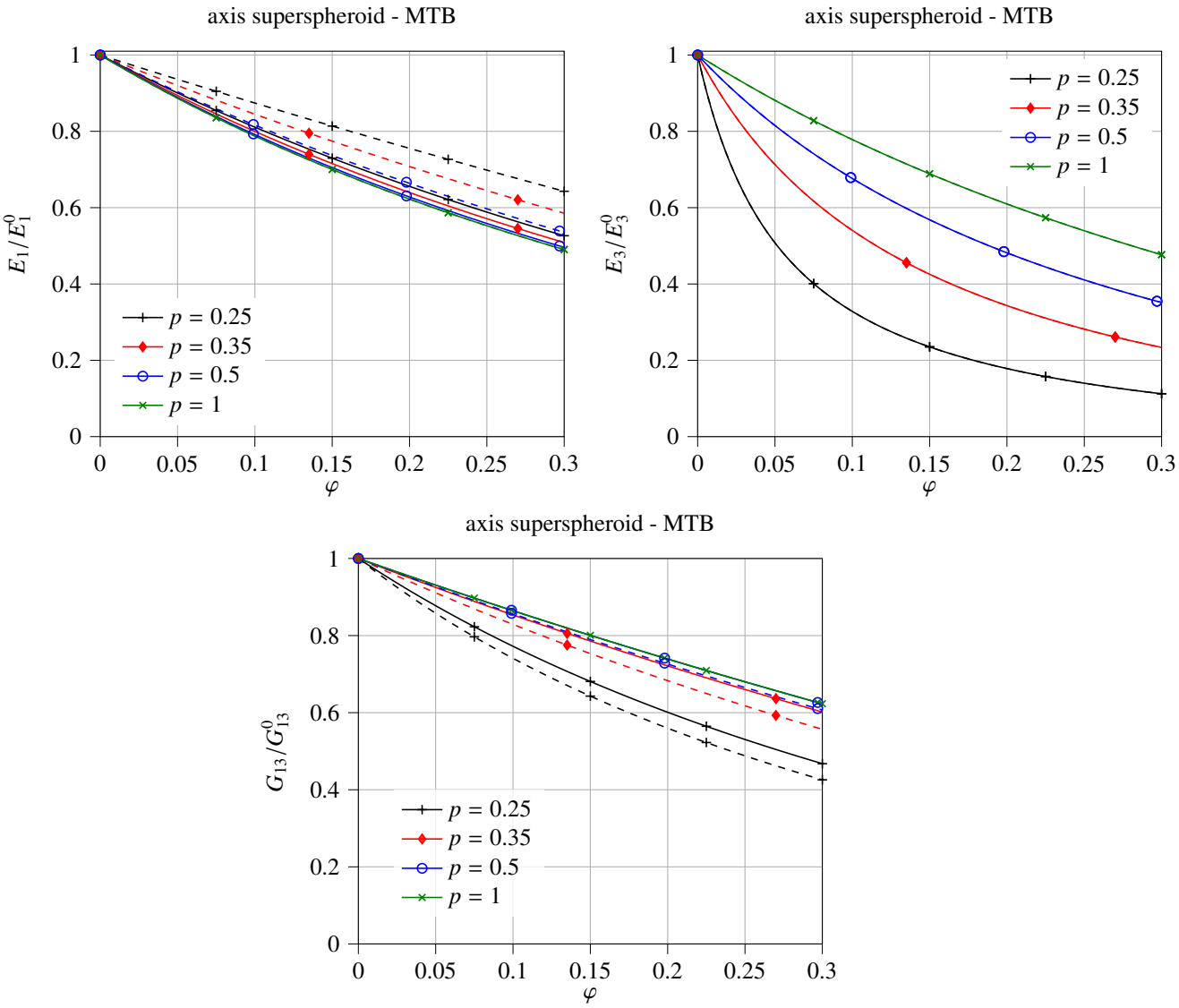


Figure 8: Effective transverse $E_1^{\mathrm{MTB}}$ (top, left) and normal $E_3^{\mathrm{MTB}}$ (top, right) Young's elastic moduli, effective axial shear modulus $G_{31}^{\mathrm{MTB}}$ as a function of porosity $\varphi$, *MTB* approximation, aligned axisymmetrical superspheroidal pores. *App 1* (plain lines): approximation formula (relations 10-11-12) for axisymmetrical spheroidal pores, *App 2* (dashed lines) : approximation *oblate spheroid with same volume* (relations 18-23). Note that the two approximations coincide only for normal Young's modulus $E_3^{\mathrm{MTB}}$.

It may be observed that:

- normal Young's modulus $E_3^{\mathrm{MTB}}$ may be estimated by a very simple approximation using compliance contribution of an oblate spheroidal pore of same volume than the axisymmetrical superspheroidal pore, in the concavity range $p < 0.5$. Numerically it is mainly related to normal component of compliance contribution tensor $H_{3333}$. Comparison between axisymmetrical superspheroidal and oblate spheroidal pores shows that both approximations lead to the same effective coefficient $E_3^{\mathrm{MTB}}$. In other words, concavity or convexity has no significant effect on this coefficient, when comparing same pores of same volume. It must be emphasized that this result is very specific and cannot be generalised. It only holds for this particular shape and the normal Young's modulus..
- oppositely, transverse Young's modulus $E_1^{\mathrm{MTB}}$ and shear coefficient $G_{31}^{\mathrm{MTB}}$ are strongly related to the concav-

ity parameter $p$. Comparison of estimates based on concave and convex pores of same volume (respectively axisymmetrical superspheroid and oblate spheroid), in the range $p < 0.5$, see figure (8), shows significant differences. This result is expected as an approximation based on an oblate spheroid of same volume is not precise for all components $H_{1111}$, $H_{1122}$, $H_{1133}$, $H_{2323}$, particularly in the concave range $0.2 < p < 0.5$. It confirms, for a $3D$ shape embedded in an anisotropic matrix that the concavity parameter is of major importance when estimating effective elastic properties.

### *4.2. Aligned axisymmetric superspheroidal pores compared with a random orientation distribution of superspherical pores in the transverse plane*

Comparisons of effective elastic moduli obtained with (*MTB*) approximation for aligned axisymmetrical superspheroidal pores and randomly oriented superspherical pores in the transverse plane are presented in figure (9). Obtained effective porous material is transversely isotropic with same symmetry axis than matrix. It may be observed that

- effects of these two shapes on elastic effective properties are strongly different in the concave range $0.2 < p < 0.5$. It is expected as the supersphere tends to three orthogonal needles (with zero volume and zero surface) when $p$ tends to zero, whereas the axisymmetrical superspheroid tends to a circular crack with one central orthogonal needle (the latter having zero volume but non zero surface).. As previously indicated, the most relevant shape compared to microstructure of porous materials is certainly supersphere.
- a significant anisotropic degree in the case of aligned axisymmetrical superspheroidal pores, in the limit $p \to 0$.

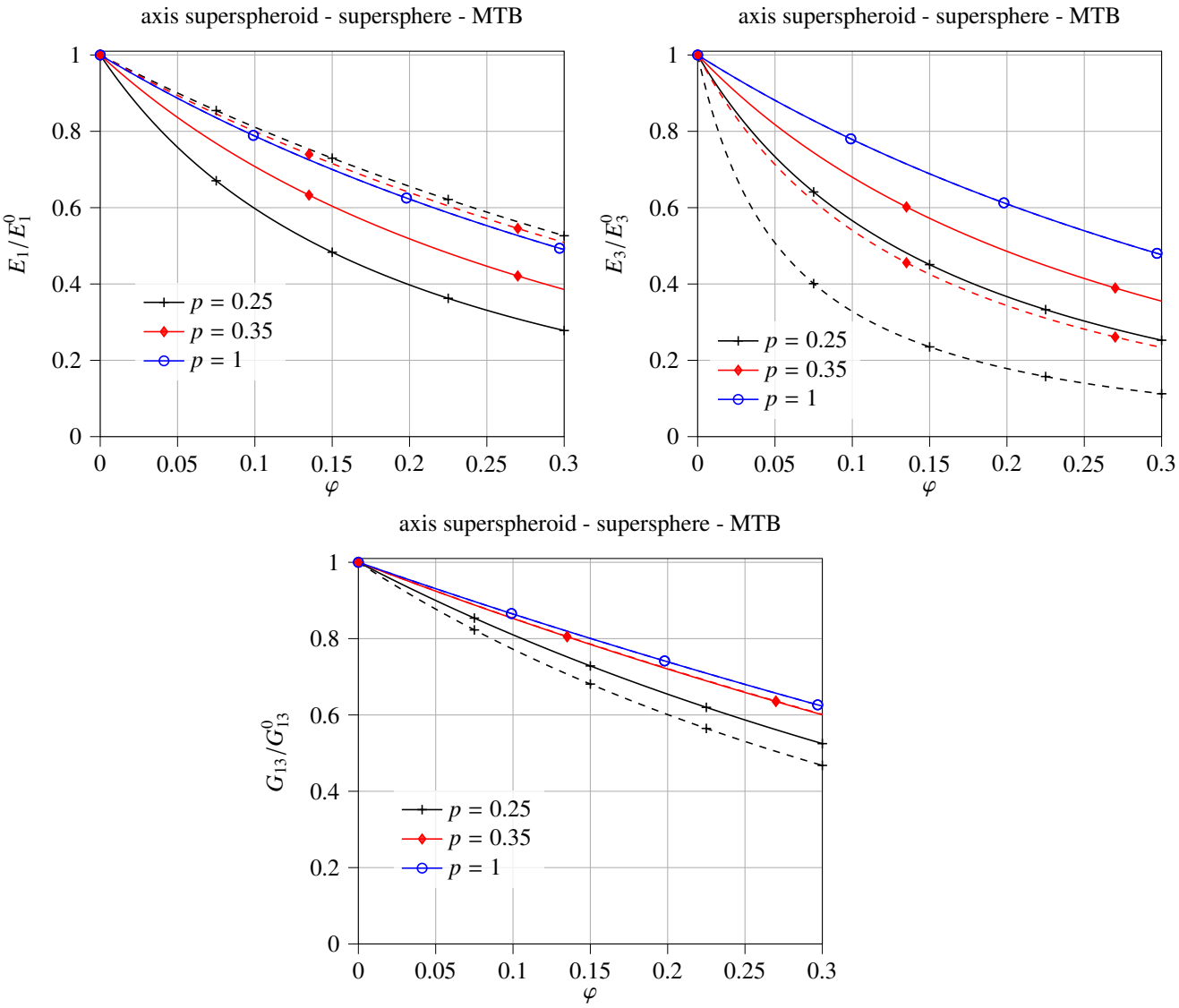


Figure 9: Effective transverse $E_1^{\mathrm{MTB}}$ (top, left) and normal $E_3^{\mathrm{MTB}}$ (top, right) Young's elastic moduli , effective shear coefficient $G_{31}^{\mathrm{MTB}}$ as a fonction of porosity $\varphi$, *MTB* approximation, superspherical (plain lines) and aligned axisymmetrical superspheroidal (dashed lines) pores.

### *4.3. Comparisons between NIA, MTB and Maxwell homogenization schemes*

Effective elastic properties predicted by Maxwell, *MTB*, *NIA* are presented in figures (10-11) for respectively for axisymmetrical superspheroidal and superspherical pores randomly oriented in transverse plane. The shape of the effective inclusion of the Maxwell scheme is still an open issue when host matrix is anisotropic (see [33, 34]). The sensitivity study on the shape of the effective inclusion, and oblate spheroid of aspect ratio $\gamma^{\Omega} = 0.5 - 1$ confirms that it is a parameter of major importance.

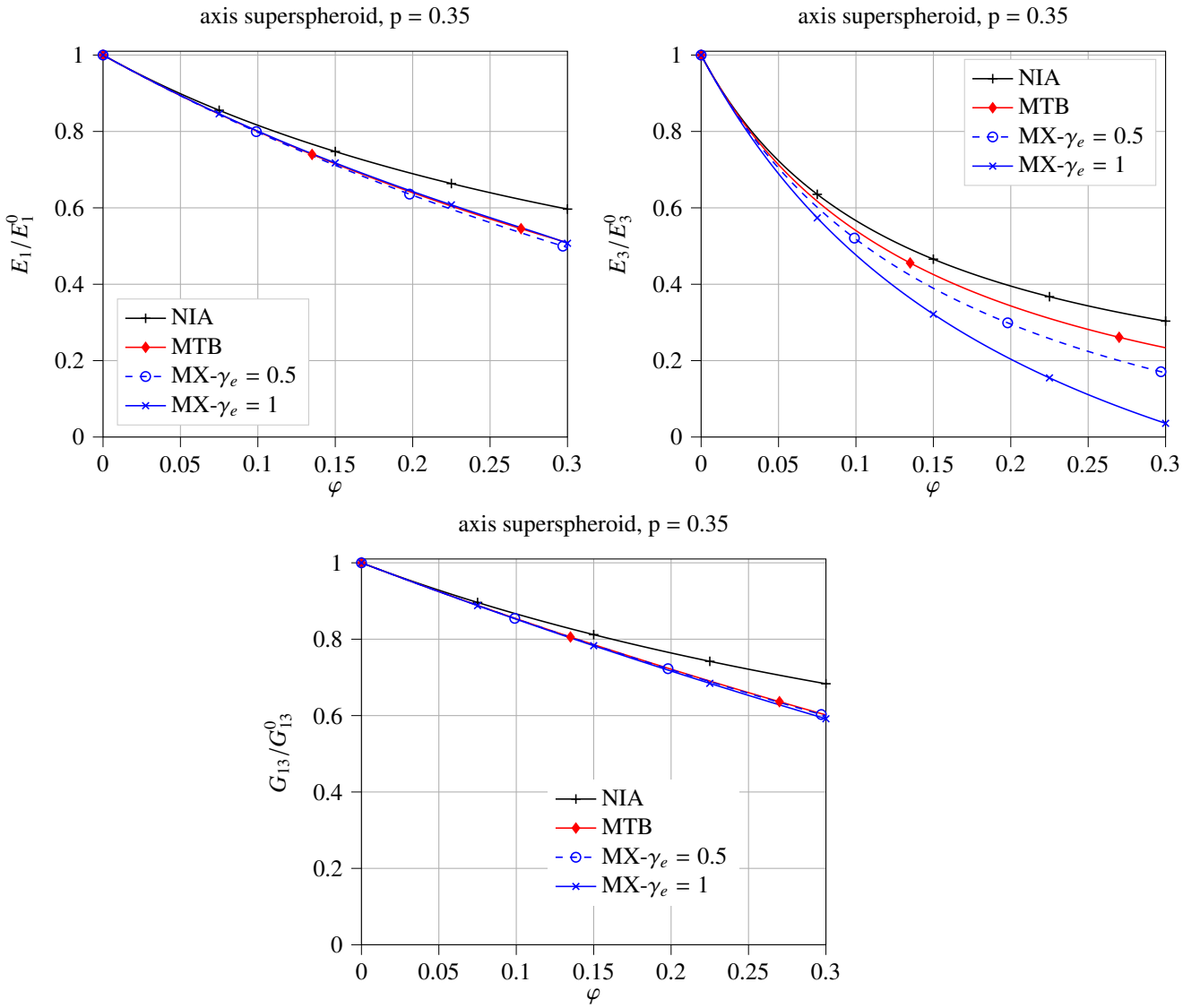


Figure 10: Effective transverse $E_1^{\text{ef}}$ (top, left) and normal $E_3^{\text{ef}}$ (top, right) Young's moduli, effective shear coefficient $G_{31}^{\text{ef}}$ (bottom) as a fonction of porosity $\varphi$, for aligned axisymmetric superspheroidal pores randomly oriented in the isotropic transverse plane.

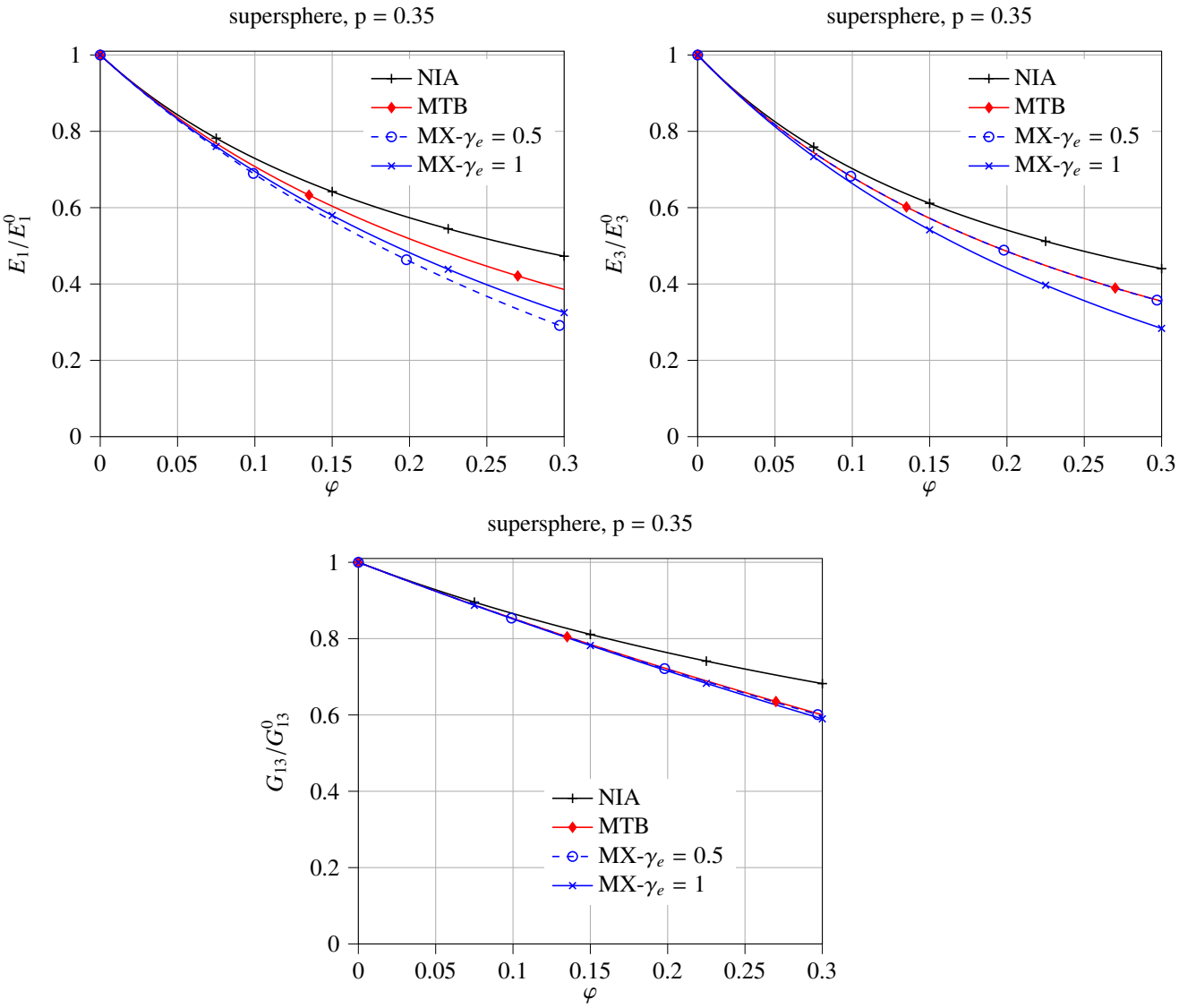


Figure 11: Effective transverse $E_1^{\text{ef}}$ (top, left) and normal $E_3^{\text{ef}}$ (top, right) Young's moduli, effective shear coefficient $G_{31}^{\text{ef}}$ (bottom) as a fonction of porosity $\varphi$, for aligned superspherical pores randomly oriented in the isotropic transverse plane.

## 5. Concluding remarks

In the present work, effective properties of a transversely-isotropic material containing concave pores are discussed and illustrated on the example of porous clay matrix. For this goal we used non-interaction approximation, Mori-Tanaka-Benveniste and Maxwell homogenization schemes. All techniques require the explicit analytical representation of the compliance contribution tensor for a single pore. These tensors were calculated for the set of superspherical and axisymmetrical superspheroidal pores with concavity parameter $p$ in the range $0.2 \leq p \leq 1$ which covers both concave ($0.2 \leq p < 0.5$) and convex shapes ($0.5 \leq p \leq 1$) using FEM. Based on the numerical solution for octahedron ($p = 0.5$) and analytical solution for sphere we built analytical approximations of the compliance contribution tensor in terms of the pore concavity parameter. The accuracy of this approximation is better than 5% for all the tensor components. We show that the concavity parameter $p$ is a parameter of major importance on the overall elastic

behavior of transversely isotropic materials containing such pore shapes. It is impossible to match effect of concave pores by oblate spheroidal pores except in the specific case of normal Young's modulus and axisymmetrical shape. The main novelty of this study is the account of concavity effects related to $3D$ shapes embedded in an anisotropic matrix while previous studies where done in the case of isotropic matrix. On the basis of presented results, it appears that it is not possible to separate effect of anisotropy from the effect of concavity to extend previous results obtained in the isotropic case. Accordingly, it is not possible to take effect of concavity from isotropic matrix and put it into TI matrix.

## 6. Acknowledgements

*JFB* thanks Cerema and Université Gustave Eiffel for allowing the creation of the joint research team entitled "Équipe de Recherche Commune sur les Matériaux pour une Construction Durable (ERC MCD)", within which these research works were carried out. *IS* acknowledges financial support from National Aeronautics and Space Administration (*NASA*) Cooperative Agreement NNX15AL51H.

## 7. Appendix. Background on tensors

Notations : Barred letters $\mathbb{A}$, $\mathbb{C}$, $\mathbb{D}$, $\mathbb{Q}$ refer to fourth order tensors, bold letters $\boldsymbol{\varepsilon}$, $\boldsymbol{\sigma}$, $\mathbf{i}$ refer to second order tensors, underlined letters $\underline{x}$, $\underline{x}$ refer to first order tensors. Einstein's summation convention over repeated indices is used unless otherwise indicated. $\otimes$, : and :: respectively represent tensor product, (dot product), contracted products on two and four indices. $\mathbf{i}$, $\mathbb{I}$, $\mathbb{J}$ and $\mathbb{K} = \mathbb{I} - \mathbb{J}$ respectively represent the second-rank identity tensor, the fourth-rank symmetric identity tensor, and fourth-rank spherical and deviatoric isotropic projectors ($\delta_{ij}$ denotes Kronecker delta symbol, $\delta_{ij} = 1$ if $i = j$, $\delta_{ij} = 0$ otherwise).

$$\underline{a} \otimes \underline{b} = a_i\, b_j\, \underline{e}_i \otimes \underline{e}_j, \quad \underline{a} \overset{s}{\otimes} \underline{b} = \frac{1}{2}\left(a_i\, b_j + a_j\, b_i\right)\, \underline{e}_i \otimes \underline{e}_j, \quad \mathbf{a} \otimes \mathbf{b} = a_{ij}\, b_{kl}\, \underline{e}_i \otimes \underline{e}_j \otimes \underline{e}_k \otimes \underline{e}_l \tag{24}$$

$$\mathbf{a} : \mathbf{b} = a_{ij}\, b_{ji}, \quad \mathbb{A} : \mathbb{B} = A_{ijop}\, B_{pokl} \underline{e}_i \otimes \underline{e}_j \otimes \underline{e}_k \otimes \underline{e}_l, \quad \mathbb{A} :: \mathbb{B} = A_{ijkl}\, B_{lkji} \tag{25}$$

$$\mathbf{a} \overline{\otimes} \mathbf{b} = \frac{1}{2}\left(a_{ik}\, b_{jl} + a_{il}\, b_{jk}\right)\, \underline{e}_i \otimes \underline{e}_j \otimes \underline{e}_k \otimes \underline{e}_l \tag{26}$$

$$\mathbb{J} = \frac{1}{3}\mathbf{i} \otimes \mathbf{i}, \quad \mathbb{I} = \mathbf{i} \overline{\otimes} \mathbf{i}, \quad \mathbf{i} = \delta_{ij} \underline{e}_i \otimes \underline{e}_j, \quad J_{ijkl} = \frac{1}{3}\delta_{ij}\,\delta_{kl}, \quad I_{ijkl} = \frac{1}{2}\left(\delta_{ik}\,\delta_{jl} + \delta_{il}\,\delta_{jk}\right) \tag{27}$$

It may be interesting to introduce standard notation and the corresponding simplified algebra for fourth-order transversely isotropic tensor (see [35]). See also post of Sébastien Brisard on github, http://sbrisard.github.io/, intitled Decomposition of transverse isotropic, fourth-rank tensors. By denoting $\underline{n}$ the unit vector of symmetry axis of the material, let us introduce the second-order tensors

$$\mathbf{i}_N = \underline{n} \otimes \underline{n} = n_i\, n_j\, \underline{e}_i \otimes \underline{e}_j \quad , \quad \mathbf{i}_T = \mathbf{i} - \mathbf{i}_N \tag{28}$$

In the particular case of $\underline{n} = \underline{e}_3$, (28) writes

$$\mathbf{i}_N = \underline{e}_3 \otimes \underline{e}_3 \quad , \quad \mathbf{i}_T = \underline{e}_1 \otimes \underline{e}_1 + \underline{e}_2 \otimes \underline{e}_2 \tag{29}$$

One introduces fourth-order tensors

$$\mathbb{E}_1 = \mathbf{i}_N \otimes \mathbf{i}_N, \quad \mathbb{E}_2 = \frac{1}{2}\mathbf{i}_T \otimes \mathbf{i}_T, \quad \mathbb{E}_3 = \frac{1}{\sqrt{2}}\mathbf{i}_N \otimes \mathbf{i}_T, \quad \mathbb{E}_4 = \frac{1}{\sqrt{2}}\mathbf{i}_T \otimes \mathbf{i}_N \tag{30}$$

$$\mathbb{E}_5 = \mathbf{i}_T \underline{\otimes} \mathbf{i}_T - \frac{1}{2}\mathbf{i}_T \otimes \mathbf{i}_T \quad , \quad \mathbb{E}_6 = \mathbf{i}_T \underline{\otimes} \mathbf{i}_N + \mathbf{i}_N \underline{\otimes} \mathbf{i}_T \tag{31}$$

It may be shown that any transversely isotropic fourth-order tensor can be decomposed as

$$\mathbb{L} = \sum_{i=1}^{6} l_i \, \mathbb{E}_i = l_i \, \mathbb{E}_i \tag{32}$$

Considering symmetry axis equal to $\underline{n} = \underline{e}_3$, Walpole matrix representation of tensor $\mathbb{H} = h_i \mathbb{E}_i$ writes

$$\boldsymbol{H} = \begin{pmatrix} \frac{h_2+h_5}{2} & \frac{h_2-h_5}{2} & \frac{h_4}{\sqrt{2}} & 0 & 0 & 0 \\ \frac{h_2-h_5}{2} & \frac{h_2+h_5}{2} & \frac{h_4}{\sqrt{2}} & 0 & 0 & 0 \\ \frac{h_3}{\sqrt{2}} & \frac{h_3}{\sqrt{2}} & h_1 & 0 & 0 & 0 \\ 0 & 0 & 0 & h_6 & 0 & 0 \\ 0 & 0 & 0 & 0 & h_6 & 0 \\ 0 & 0 & 0 & 0 & 0 & h_5 \end{pmatrix} \tag{33}$$

Relations with usual $H_{ijkl}$ components write

$$h_1 = H_{3333}, \quad h_2 = H_{1111} + H_{1122}, \quad h_3 = \sqrt{2} H_{3311}, \quad h_4 = \sqrt{2} H_{1133}, \quad h_5 = H_{1111} - H_{1122}, \quad h_6 = 2 H_{2323} \tag{34}$$

We detail herefafter calculation of compliance contribution $\mathbb{H}_0^{\mathcal{E}}$ of a spheroidal pore $\mathcal{E}$ in *TI* basis, in terms of components $c_i$ and $p_i$ of matrix stiffness tensor $\mathbb{C}_0$ and strain Hill polarisation tensor $\mathbb{P}_0^{\mathcal{E}}$

$$\mathbb{H}_0^{\mathcal{E}} = \left(\mathbb{Q}_0^{\mathcal{E}}\right)^{-1}, \quad \mathbb{Q}_0^{\mathcal{E}} = \sum_{i=1}^{6} q_i \, \mathbb{E}_i, \quad \mathbb{P}_0^{\mathcal{E}} = \sum_{i=1}^{6} p_i \, \mathbb{E}_i, \quad \mathbb{C}_0 = \sum_{i=1}^{6} c_i \, \mathbb{E}_i, \quad q_4 = q_3, \quad p_4 = p_3, \quad c_4 = c_3 \tag{35}$$

$$q_1 = c_1 - c_1^2 p_1 - c_3^2 p_2 - 2\, c_1\, c_3\, p_3, \quad q_2 = c_2 - c_3^2 p_1 - c_2^2 p_2 - 2\, c_2\, c_3\, p_3 \tag{36}$$

$$q_4 = q_3 = c_3 - c_1\, c_3\, p_1 - c_2\, c_3\, p_2 - \left(c_1\, c_2 + c_3^2\right) p_3 \tag{37}$$

$$q_5 = c_5\,(1 - c_5\, p_5)\,, \quad q_6 = c_6\,(1 - c_6\, p_6) \tag{38}$$

and components $h_i$ of compliance contribution tensor are deduced from calculation rules in transversely isotropic basis (with $q_4 = q_3$)

$$\begin{pmatrix} h_1 & h_3 \\ h_4 & h_2 \end{pmatrix} = \begin{pmatrix} q_1 & q_3 \\ q_3 & q_2 \end{pmatrix}^{-1} = \frac{1}{q_1\, q_2 - q_3^2} \begin{pmatrix} q_2 & -q_3 \\ -q_3 & q_1 \end{pmatrix}, \quad h_i = \frac{1}{q_i} = \frac{1}{c_i\,(1 - c_i\, p_i)} \quad (i = 5, 6) \tag{39}$$

See similar derivations in [16] , with different *TI* tensor basis (see formula 2.56).

A fourth order tensor $\mathbb{T}$ may be *transversely isotropised* by projection onto a transversely isotropic basis to obtain $\Pi^{TI}(\mathbb{T})$

$$\Pi^{TI}(\mathbb{T}) = \sum_{i=1}^{2} (\mathbb{E}_i :: \mathbb{T})\, \mathbb{E}_i + (\mathbb{E}_4 :: \mathbb{T})\, \mathbb{E}_3 + (\mathbb{E}_3 :: \mathbb{T})\, \mathbb{E}_4 + \frac{1}{2} \sum_{i=5}^{6} (\mathbb{E}_i :: \mathbb{T})\, \mathbb{E}_i \tag{40}$$

In case of a symmetry axis is $x_3$, we apply the transformation $\boldsymbol{Q}^{\alpha}$ representing a rotation of angle $\varphi$ about $x_3$ axis to fourth order tensor $\mathbb{T}$

$$T^{\alpha}_{ijkl} = Q^{\alpha}_{ip} Q^{\alpha}_{jq} Q^{\alpha}_{kr} Q^{\alpha}_{ls} T_{pqrs} \tag{41}$$

with

$$\underline{e}^{\alpha}_1 = \cos(\varphi)\underline{e}_1 + \sin(\varphi)\,\underline{e}_2, \quad \underline{e}^{\alpha}_2 = -\sin(\varphi)\underline{e}_1 + \cos(\varphi)\,\underline{e}_2, \quad \underline{e}^{\alpha}_3 = \underline{e}_3 \tag{42}$$

and non zero components of matrix $\boldsymbol{Q}^{\alpha}$ write

$$Q^{\alpha}_{11} = Q^{\alpha}_{22} = \cos(\varphi), \quad Q^{\alpha}_{12} = -Q^{\alpha}_{21} = \sin(\varphi), \quad Q^{\alpha}_{33} = 1 \tag{43}$$

Transverse isotropic projection $\Pi^{TI}(\mathbb{T})$ (40) corresponds to the following average over orientations, in the transverse plane $x_1 - x_2$

$$\left[\Pi^{TI}(\mathbb{T})\right]_{ijkl} = \frac{1}{2\pi}\int_0^{2\pi} T^{\alpha}_{ijkl}(\varphi)\, d\varphi = \frac{1}{2\pi}\int_0^{2\pi} Q^{\alpha}_{ip}(\varphi)\, Q^{\alpha}_{jq}(\varphi)\, Q^{\alpha}_{kr}(\varphi)\, Q^{\alpha}_{ls}(\varphi)\, T_{pqrs}\, d\varphi \tag{44}$$

Compliance contribution tensor of a superspherical pore aligned with the directions of symmetry of a transversely isotropic matrix (with $x_3$ symmetry axis of matrix) is tetragonal, with 6 independent components $H_{1111}$, $H_{1122}$, $H_{1133}$, $H_{3333}$, $H_{1212}$, and $H_{2323}$. Average compliance contribution tensor related to an isotropic orientation distribution of superspherical pores in the transverse isotropic plane $x_1 - x_2$ is transversely isotropic and obtained by transverse isotropic projection

$$\begin{aligned} &h^{TI}_1 = H_{3333}, \quad h^{TI}_2 = H_{1111} + H_{1122}, \quad h^{TI}_3 = h^{TI}_4 = \sqrt{2}\, H_{1133} \\ &h^{TI}_5 = \frac{H_{1111} - H_{1122} + 2H_{1212}}{2}, \quad h^{TI}_6 = 2H_{2323} \end{aligned} \tag{45}$$

$$\begin{aligned} &H^{TI}_{1111} = \frac{3\,H_{1111} + H_{1122} + 2\,H_{1212}}{4}, \quad H^{TI}_{1122} = \frac{H_{1111} + 3\,H_{1122} - 2\,H_{1212}}{4} \\ &H^{TI}_{1133} = H_{1133}, \quad H^{TI}_{3333} = H_{3333}, \quad H^{TI}_{2323} = H_{2323}, \quad H^{TI}_{1212} = \frac{H_{1111} - H_{1122} + 2\,H_{1212}}{4} \end{aligned} \tag{46}$$

By using euclidean norm $\|\mathbb{H}\| = \left(H_{ijkl}\, H_{ijkl}\right)^{1/2}$ the relative distance between a tetragonal tensor and its transverse isotropic projection writes

$$\frac{\left\|\left(\mathbb{H}^{\text{tetragonal}} - \Pi^{TI}\left(\mathbb{H}^{\text{tetragonal}}\right)\right)\right\|}{\left\|\mathbb{H}^{\text{tetragonal}}\right\|} = \frac{1}{\sqrt{2}}\frac{|H_{1111} - H_{1122} - 2\,H_{1212}|}{\left(2\left(H^2_{1111} + H^2_{1122} + 2\left(H^2_{1133} + H^2_{1212} + 2H^2_{2323}\right)\right) + H^2_{3333}\right)^{1/2}} \tag{47}$$

## 8. Appendix. Background on property contribution tensors

Property contribution tensors are used in micromechanics to describe the contribution of a single inhomogeneity to the property of interest ([26]). Compliance contribution tensors have been first introduced in the context of pores and cracks by [36] as the extra average strain produced by a pore. The average strain, over representative volume $|\,\Omega\,|$, can be represented as a sum

$$\boldsymbol{\varepsilon} = \mathbb{S}_0 : \boldsymbol{\Sigma} + \Delta\boldsymbol{\varepsilon} \tag{48}$$

where $\mathbb{S}_0$ where is the compliance tensor of the matrix and $\boldsymbol{\Sigma}$ is uniform remotely applied stress. The material is assumed to be a linear elastic; hence, the extra strain $\Delta\boldsymbol{\varepsilon}$ due to presence of an inhomogeneity $\mathcal{E}$ is a linear function of the applied stress:

$$\Delta\boldsymbol{\varepsilon} = f\,\mathbb{H}^{\mathcal{E}}_0 : \boldsymbol{\Sigma}, \quad \text{with } f = \frac{|\,\mathcal{E}\,|}{|\,\Omega\,|} \tag{49}$$

where $|\ \mathcal{E}\ |$ is the pore volume and $\mathbb{H}_0^{\mathcal{E}}$ is fourth-rank compliance contribution tensor of the pore. The $\mathbb{H}_0^{\mathcal{E}}$ tensor is determined by the shape and size of the inhomogeneity, as well as properties of the matrix and of the inhomogeneity material. This tensor is also affected by elastic interactions. In the non-interaction approximation, it is taken by treating the inhomogeneities as isolated ones. In the case of multiple inhomogeneities, the extra strain produced by *m-th* inhomogeneity is $\Delta\boldsymbol{\varepsilon}^{(m)} = f^{(m)}\,\mathbb{H}_0^{\mathcal{E}(m)} : \boldsymbol{\Sigma}$ so that the extra compliance due to all the inhomogeneities is given by

$$\Delta\boldsymbol{\varepsilon} = \left[\sum f^{(m)}\,\mathbb{H}_0^{\mathcal{E}(m)}\right] : \boldsymbol{\Sigma} \tag{50}$$

Formula (50) highlights the fundamental importance of the compliance contribution tensors: these tensors have to be summed up and averaged in the context of the effective elastic properties. The sum

$$\sum f^{(m)}\,\mathbb{H}_0^{\mathcal{E}(m)} \tag{51}$$

properly reflects compliance contributions of individual inhomogeneities and constitutes the general microstructural parameters in whose terms the effective compliance should be expressed. Components of this tensor were calculated for $2-D$ pores of various shape and $3-D$ ellipsoidal pores in isotropic material by [2]. For the general case of elastic inhomogeneities, these tensors were introduced and calculated (for ellipsoidal shapes) by Sevostianov and Kachanov ([37]). Components of the compliance contribution tensor for various concave pores in isotropic matrix have been calculated by [10] (supersphere), [38] (axisymmetric pore obtained by rotation of a supersphere around one of its principal diagonals), [11] (combined effect of concavity and aspect ratio), and [39] (tetrahedron-like pores). [16, 28] calculated components of this tensor for a spheroidal inhomogeneity embedded in a transversely-isotropic material.

We recall the compact solution of strain Hill polarization tensor of a spheroidal inclusion aligned in a transversely isotropic host matrix recently presented in [28] (reader may refer to this reference for the detailed derivation and python script of the complete solution). The corresponding compliance contribution tensor may be deduced from relations presented in section (7). In what follows, the aspect ratio of the spheroidal inclusion is denoted $\omega$, and the symmetry axis $\underline{n}$ of the host matrix and the spheroidal inclusion is taken as $\underline{n} = \underline{e}_3$. The particular case of the spherical pore is then deduced by setting $\omega = 1$. The solution writes in Walpole *TI* tensor basis

$$\mathbb{P} = p_1\,\mathbb{E}_1 + p_2\,\mathbb{E}_2 + p_3\,(\mathbb{E}_3 + \mathbb{E}_4) + p_5\,\mathbb{E}_5 + p_6\,\mathbb{E}_6 \tag{52}$$

with

$$\begin{cases}
p_1 = \dfrac{(C_{2323} - \omega^2\,C_{1111})\,\mathcal{J}_4 + \omega^2\,C_{1111}\,\mathcal{J}_2}{2\,C_{2323}\,C_{3333}} & \text{(53a)}\\[2ex]
p_2 = \omega^2\,\dfrac{(\omega^2\,C_{2323} - C_{3333})\,\mathcal{J}_4 + (C_{3333} - 2\,\omega^2\,C_{2323})\,\mathcal{J}_2 + \omega^2\,C_{2323}\,\mathcal{J}_0}{4\,C_{2323}\,C_{3333}} & \text{(53b)}\\[2ex]
p_3 = p_4 = \dfrac{\omega^2\,(C_{2323} + C_{1133})\,(\mathcal{J}_4 - \mathcal{J}_2)}{2\sqrt{2}\;C_{2323}\,C_{3333}} & \text{(53c)}\\[2ex]
p_5 = \dfrac{p_2}{2} + \dfrac{\omega^2\,(\mathcal{I}_0 - \mathcal{I}_2)}{8\,C_{2323}} & \text{(53d)}\\[2ex]
p_6 = \dfrac{(\omega^4\,C_{1111} + C_{3333} + 2\,\omega^2\,C_{1133})\,\mathcal{J}_4 - 2\,\omega^2\,(\omega^2\,C_{1111} + C_{1133})\,\mathcal{J}_2 + \omega^4\,C_{1111}\,\mathcal{J}_0}{8\,C_{2323}\,C_{3333}} + \dfrac{\mathcal{I}_2}{8\,C_{2323}} & \text{(53e)}
\end{cases}$$

with

$$\mathcal{J}_k = \mathcal{J}_k(\omega\,\gamma_1, \omega\,\gamma_2) \quad (k \in \{0, 2, 4\}) \quad \text{and} \quad \mathcal{I}_k = \mathcal{I}_k(\omega\,\gamma_3) \quad (k \in \{0, 2\}) \tag{54}$$

$$\gamma_3 = \sqrt{\frac{C_{1111} - C_{1122}}{2\,C_{2323}}} \tag{55}$$

$\gamma_1$ and $\gamma_2$ denote the square roots of the roots of the polynomial

$$Z^2\,C_{2323}\,C_{3333} + Z\,(C_{1133}^2 + 2\,C_{1133}\,C_{2323} - C_{1111}\,C_{3333}) + C_{1111}\,C_{2323} = 0 \tag{56}$$

$$\gamma_1 = \sqrt{\frac{C_{1111}\,C_{3333} - C_{1133}^2 - 2\,C_{1133}\,C_{2323} + \sqrt{\Delta}}{2\,C_{2323}\,C_{3333}}}\;;\; \gamma_2 = \sqrt{\frac{C_{1111}\,C_{3333} - C_{1133}^2 - 2\,C_{1133}\,C_{2323} - \sqrt{\Delta}}{2\,C_{2323}\,C_{3333}}} \tag{57}$$

with

$$\Delta = (C_{1111}\,C_{3333} - C_{1133}^2)\,(C_{1111}\,C_{3333} - C_{1133}^2 - 4\,C_{1133}\,C_{2323} - 4\,C_{2323}^2) \tag{58}$$

The square root of a complex argument is defined with a positive real part and it is consistent with the `cmath` library of `Python`. The inverse hyperbolic cosine of a complex argument, denoted by arcosh , has one branch cut, extending left from 1 along the real axis to $-\infty$, continuous from above. Note that $\operatorname{arcosh} Z = \ln\left(Z + \sqrt{Z^2-1}\right)$ where the principal value of the logarithm is chosen such that the imaginary part has the smallest value and belongs to $]-\frac{\pi}{2}, \frac{\pi}{2}]$ with the same branch cut as the square root.

$$\mathcal{I}_k(\eta) = \int_{z=-1}^{1} \frac{z^k}{z^2 + \eta^2\,(1-z^2)}\,\mathrm{d}z \quad \text{and} \quad \mathcal{J}_k(\eta_1,\eta_2) = \int_{z=-1}^{1} \frac{z^k}{\left(z^2 + \eta_1^2\,(1-z^2)\right)\left(z^2 + \eta_2^2\,(1-z^2)\right)}\,\mathrm{d}z \tag{59}$$

| | $\mathcal{I}_0(\eta)$ | $\mathcal{I}_2(\eta)$ | $\mathcal{I}_4(\eta)$ |
|---|---|---|---|
| if $\eta = 1$ | $2$ | $\frac{2}{3}$ | $\frac{2}{5}$ |
| if $\eta \neq 1$ | $2\,\frac{\operatorname{arcosh}\eta}{\eta\sqrt{\eta^2-1}}$ | $2\,\frac{\eta\,\operatorname{arcosh}\eta - \sqrt{\eta^2-1}}{(\eta^2-1)^{\frac{3}{2}}}$ | $\frac{2}{3}\,\frac{3\,\eta^3\,\operatorname{arcosh}\eta + (1-4\,\eta^2)\,\sqrt{\eta^2-1}}{(\eta^2-1)^{\frac{5}{2}}}$ |

Table 5: Calculation of integrals $\mathcal{I}_k(\eta)$

| | $\mathcal{J}_0(\eta_1,\eta_2)$ | $\mathcal{J}_2(\eta_1,\eta_2)$ | $\mathcal{J}_4(\eta_1,\eta_2)$ |
|---|---|---|---|
| if $\eta_1 = \eta_2 = 1$ | $2$ | $\frac{2}{3}$ | $\frac{2}{5}$ |
| if $\eta_1 = \eta_2 \neq 1$ | $\frac{\operatorname{arcosh}\eta_1 + \eta_1\sqrt{\eta_1^2-1}}{\eta_1^3\sqrt{\eta_1^2-1}}$ | $\frac{\eta_1\sqrt{\eta_1^2-1} - \operatorname{arcosh}\eta_1}{\eta_1\,(\eta_1^2-1)^{\frac{3}{2}}}$ | $\frac{(2+\eta_1^2)\sqrt{\eta_1^2-1} - 3\,\eta_1\,\operatorname{arcosh}\eta_1}{(\eta_1^2-1)^{\frac{5}{2}}}$ |
| if $\eta_1 \neq \eta_2$ | $\frac{(\eta_1^2-1)\,\mathcal{I}_0(\eta_1) - (\eta_2^2-1)\,\mathcal{I}_0(\eta_2)}{\eta_2^2-\eta_1^2}$ | $\frac{(\eta_1^2-1)\,\mathcal{I}_2(\eta_1) - (\eta_2^2-1)\,\mathcal{I}_2(\eta_2)}{\eta_2^2-\eta_1^2}$ | $\frac{(\eta_1^2-1)\,\mathcal{I}_4(\eta_1) - (\eta_2^2-1)\,\mathcal{I}_4(\eta_2)}{\eta_2^2-\eta_1^2}$ |

Table 6: Calculation of integrals $\mathcal{J}_k(\eta)$

Related compliance contribution of the spheroidal pore is then deduced from relations (35-39).

The exact solution of compliance contribution tensor of the penny shaped crack, $\mathbb{H} = \lim_{\omega\to 0}\,\omega\,(\mathbb{Q}_0)^{-1}$, is detailed in [28]. We only recall final results. One uses

$$\begin{cases}
p_1^1 = \dfrac{\pi}{2\,(\gamma_1+\gamma_2)}\,\dfrac{C_{1111} - (\gamma_1^2 + \gamma_1\,\gamma_2 + \gamma_2^2)\,C_{2323}}{C_{2323}\,C_{3333}} & \text{(60a)}\\
p_2^1 = \dfrac{\pi}{4\,(\gamma_1+\gamma_2)}\,\left(\dfrac{1}{\gamma_1\,\gamma_2\,C_{3333}} + \dfrac{1}{C_{2323}}\right) & \text{(60b)}\\
p_3^1 = -\,\dfrac{\sqrt{2}\,\pi}{4\,(\gamma_1+\gamma_2)}\,\dfrac{C_{1133} + C_{2323}}{C_{2323}\,C_{3333}} & \text{(60c)}\\
p_5^1 = \dfrac{\pi}{8}\,\left(\dfrac{1}{\gamma_1\,\gamma_2\,(\gamma_1+\gamma_2)\,C_{3333}} + \left(\dfrac{1}{\gamma_1+\gamma_2} + \dfrac{1}{\gamma_3}\right)\,\dfrac{1}{C_{2323}}\right) & \text{(60d)}\\
p_6^1 = \dfrac{\pi}{8}\,\left(\dfrac{C_{1111} - 2\,\gamma_1\,\gamma_2\,C_{1133} - \gamma_1\,\gamma_2\,(\gamma_1^2 + \gamma_1\,\gamma_2 + \gamma_2^2)\,C_{3333}}{\gamma_1\,\gamma_2\,(\gamma_1+\gamma_2)\,C_{2323}\,C_{3333}} - \dfrac{\gamma_3}{C_{2323}}\right) & \text{(60e)}
\end{cases}$$

$\gamma_1$, $\gamma_2$, $\gamma_3$ have been previously defined. Compliance contribution tensor of a penny shaped crack aligned in a transversely isotropic host matrix writes

$$\mathbb{H} = \lim_{\omega\to 0} \omega\,(\mathbb{Q}_0)^{-1} = -\frac{1}{C_{3333}^2\,p_1^1 + 2\,C_{1133}^2\,p_2^1 + 2\,\sqrt{2}\,C_{3333}\,C_{1133}\,p_3^1}\,\mathbb{E}_1 - \frac{1}{4\,C_{2323}^2\,p_6^1}\,\mathbb{E}_6 \tag{61}$$

where $p_1^1$, $p_2^1$, $p_3^1$ and $p_6^1$ are given in (60a), (60b), (60c) and (60e). One deduces the components denoted $h_1^c$, $h_6^c$ and used in approximate relations of compliance contribution tensor of an aligned axisymmetric superspheroidal pore:

$$h_1^c = -\frac{1}{C_{3333}^2\,p_1^1 + 2\,C_{1133}^2\,p_2^1 + 2\,\sqrt{2}\,C_{3333}\,C_{1133}\,p_3^1}, \quad h_6^c = -\frac{1}{4\,C_{2323}^2\,p_6^1} \tag{62}$$

## 9. Appendix: numerical results for approximation formula of compliance contribution tensors

Finite element results of a superspherical pore embedded in a *TI* matrix, are given in table 4 of paper [24], and recalled in table (7).

| $p$ | $H^{\mathcal{E}}_{1111}$ | $H^{\mathcal{E}}_{3333}$ | $H^{\mathcal{E}}_{1122}$ | $H^{\mathcal{E}}_{1133}$ | $H^{\mathcal{E}}_{1212}$ | $H^{\mathcal{E}}_{1313}$ |
|---|---|---|---|---|---|---|
| 0.2 | 0.5401 | 0.9682 | -0.1386 | -0.1093 | 0.2043 | 0.4972 |
| 0.25 | 0.3391 | 0.6106 | -0.0895 | -0.0676 | 0.1288 | 0.3327 |
| 0.3 | 0.2521 | 0.4567 | -0.0682 | -0.0496 | 0.0984 | 0.2715 |
| 0.35 | 0.2052 | 0.3749 | -0.0567 | -0.0400 | 0.0844 | 0.2454 |
| 0.4 | 0.1770 | 0.3269 | -0.0497 | -0.0343 | 0.0779 | 0.2330 |
| 0.45 | 0.1589 | 0.2967 | -0.0450 | -0.0308 | 0.0749 | 0.2265 |
| 0.5 | 0.1460 | 0.2747 | -0.0413 | -0.0284 | 0.0735 | 0.2229 |
| 0.6 | 0.1337 | 0.2542 | -0.0371 | -0.0263 | 0.0727 | 0.2199 |
| 0.7 | 0.1269 | 0.2419 | -0.0342 | -0.0252 | 0.0728 | 0.2194 |
| 0.8 | 0.1229 | 0.2345 | -0.0321 | -0.0246 | 0.0731 | 0.2200 |
| 0.9 | 0.1204 | 0.2297 | -0.0305 | -0.0242 | 0.0735 | 0.2212 |
| 1 | 0.1188 | 0.2266 | -0.0293 | -0.0239 | 0.0740 | 0.2226 |

Table 7: Numerical estimation of $H^{\mathcal{E}}_{ijkl}$ for the superspheroidal pore embedded in a transversely isotropic corrected model with different values of concavity $p \in [0.2, 1]$, from [24].

Approximate relations for the concavity parameter range $0.2 < p < 1$ write

$$\begin{aligned}
f^{\text{se-a}}_{1111}(p) &= 2.72394p^2 - 2.6248p + 1.63141\\
f^{\text{se-a}}_{1122}(p) &= 1.23332p^2 - 1.20253p + 1.29293\\
f^{\text{se-a}}_{1133}(p) &= 3.75077p^2 - 3.50795p + 1.81628\\
f^{\text{se-a}}_{3333}(p) &= 2.77572p^2 - 2.46747p + 1.5398\\
f^{\text{se-a}}_{1212}(p) &= 17.1508p^4 - 43.7713p^3 + 38.3878p^2 - 13.1282p + 2.36576\\
f^{\text{se-a}}_{2323}(p) &= 50.3296p^4 - 90.0984p^3 + 59.3072p^2 - 15.8086p + 2.1938
\end{aligned} \tag{63}$$

$$
\begin{aligned}
f_{1111}^{\text{se-b}}(p) &= -0.197702p^2 + 0.220097p + 0.939377 \\
f_{1122}^{\text{se-b}}(p) &= -0.24264p^2 + 0.0415192p + 1.0399 \\
f_{1133}^{\text{se-b}}(p) &= -0.357454p^2 + 0.52452p + 0.827103 \\
f_{3333}^{\text{se-b}}(p) &= -0.326089p^2 + 0.439731p + 0.861657 \\
f_{1212}^{\text{se-b}}(p) &= -2.04372p^4 + 7.78585p^3 - 11.3964p^2 + 7.68465p - 0.839061 \\
f_{2323}^{\text{se-b}}(p) &= -2.65601p^4 + 9.6441p^3 - 13.4224p^2 + 8.59804p - 0.982841
\end{aligned}
\tag{64}
$$

Finite element results of an axisymmetrical superspheroidal pore embedded in a *TI* matrix are given in table 3 of paper [24] and recalled in table (8).

| $p$ | $H^{\mathcal{E}}_{1111}$ | $H^{\mathcal{E}}_{1122}$ | $H^{\mathcal{E}}_{1133}$ | $H^{\mathcal{E}}_{3333}$ | $H^{\mathcal{E}}_{1212}$ | $H^{\mathcal{E}}_{1313}$ | $\frac{H^{\mathcal{E}}_{1111}-H^{\mathcal{E}}_{1122}}{2}$ | Error$_{1212}$[1] |
|---|---|---|---|---|---|---|---|---|
| 0.2 | 0.1004 | -0.0192 | -0.0520 | 3.6670 | 0.0597 | 0.8424 | 0.0598 | 0.16% |
| 0.25 | 0.1026 | -0.0212 | -0.0442 | 1.5948 | 0.0619 | 0.4132 | 0.0619 | 0.04% |
| 0.3 | 0.1068 | -0.0232 | -0.0395 | 0.9354 | 0.0650 | 0.2928 | 0.0650 | 0.01% |
| 0.35 | 0.1102 | -0.0248 | -0.0359 | 0.6445 | 0.0675 | 0.2495 | 0.0675 | 0.00% |
| 0.4 | 0.1128 | -0.0260 | -0.0331 | 0.4929 | 0.0694 | 0.2324 | 0.0694 | 0.00% |
| 0.45 | 0.1147 | -0.0270 | -0.0310 | 0.4047 | 0.0708 | 0.2248 | 0.0708 | 0.00% |
| 0.5 | 0.1159 | -0.0276 | -0.0293 | 0.3492 | 0.0718 | 0.2211 | 0.0718 | 0.00% |
| 0.6 | 0.1175 | -0.0284 | -0.0271 | 0.2900 | 0.0730 | 0.2187 | 0.0730 | 0.01% |
| 0.7 | 0.1182 | -0.0288 | -0.0258 | 0.2604 | 0.0735 | 0.2188 | 0.0735 | 0.01% |
| 0.8 | 0.1186 | -0.0291 | -0.0249 | 0.2436 | 0.0738 | 0.2197 | 0.0738 | 0.01% |
| 0.9 | 0.1187 | -0.0292 | -0.0243 | 0.2333 | 0.0739 | 0.2211 | 0.0739 | 0.01% |
| 1 | 0.1187 | -0.0293 | -0.0239 | 0.2265 | 0.0740 | 0.2226 | 0.0740 | 0.01% |

[1] Relative error of $\frac{H^{\mathcal{E}}_{1111}-H^{\mathcal{E}}_{1122}}{2}$ with respect to $H^{\mathcal{E}}_{1212}$

Table 8: Numerical estimation of $H^{\mathcal{E}}_{ijkl}$ for the superspheroidal pore embedded in a transversely isotropic corrected model with different values of concavity $p \in [0.2, 1]$, from [24].

Approximate relations for the concavity parameter range $0.2 < p < 1$ write

$$
\begin{aligned}
f_{1111}^{\text{so-a}}(p) &= 54.285p^4 - 85.8182p^3 + 44.7893p^2 - 6.31294p + 0.294191 \\
f_{1122}^{\text{so-a}}(p) &= 50.5731p^4 - 84.3085p^3 + 46.7634p^2 - 7.38197p + 0.378348 \\
f_{1133}^{\text{so-a}}(p) &= 39.0659p^4 - 42.9843p^3 + 7.43095p^2 + 5.44332p - 0.646506
\end{aligned}
\tag{65}
$$

$$
\begin{aligned}
f_{1111}^{\text{so-b}}(p) &= -3.74036p^4 + 13.3244p^3 - 18.0592p^2 + 11.0818p - 1.45743 \\
f_{1122}^{\text{so-b}}(p) &= -4.07865p^4 + 14.7289p^3 - 20.227p^2 + 12.5889p - 1.82352 \\
f_{1133}^{\text{sp-b}}(p) &= -1.92702p^4 + 6.39843p^3 - 7.8095p^2 + 3.95979p + 0.293327
\end{aligned}
\tag{66}
$$

## 10. References

## References


[1] J. D. Eshelby, Elastic inclusions and inhomogeneities, in: Progress in Solid Mechanics 2, I.N. Sneddon and R. Hill Editors, North-Holland, Amsterdam, 1961, pp. 89–140.

[2] M. Kachanov, I. Tsukrov, B. Shafiro, Effective Moduli of Solids With Cavities of Various Shapes, ASME. Applied Mechanics Review 47 (1) (1994) S151–S174.

[3] S. Krasnitskii, A. Trofimov, E. Radi, I. Sevostianov, Effect of a rigid toroidal inhomogeneity on the elastic properties of a composite, Mathematics and Mechanics of Solids 24 (4) (2019) 1129 – 1146.

[4] E. J. Garboczi, J. F. Douglas, Elastic moduli of composites containing a low concentration of complex-shaped particles having a general property contrast with the matrix, Mechanics of Materials 51 (2012) 53 – 65.

[5] H. J. Böhm, A. Rasool, Effects of particle shape on the thermoelastoplastic behavior of particle reinforced composites, International Journal of Solids and Structures 87 (2016) 90 – 101.

[6] B. Drach, A. Drach, I. Tsukrov, Prediction of the effective elastic moduli of materials with irregularly-shaped pores based on the pore projected areas, International Journal of Solids and Structures 51 (14) (2014) 2687 – 2695.

[7] B. Drach, I. Tsukrov, A. Trofimov, Comparison of full field and single pore approaches to homogenization of linearly elastic materials with pores of regular and irregular shapes, International Journal of Solids and Structures 96 (2016) 48 – 63.

[8] A. Trofimov, B. Drach, I. Sevostianov, Effective elastic properties of composites with particles of polyhedral shapes, International Journal of Solids and Structures 120 (2017) 157 – 170.

[9] T. I. Zohdi, Genetic design of solids possessing a random-particulate microstructure, Philosophical Transactions of the Royal Society of London. Series A: Mathematical, Physical and Engineering Sciences 361 (1806) (2003) 1021–1043.

[10] F. Chen, I. Sevostianov, A. Giraud, D. Grgic, Evaluation of the effective elastic and conductive properties of a material containing concave pores, International Journal of Engineering Science 97 (2015) 60 – 68.

[11] F. Chen, I. Sevostianov, A. Giraud, D. Grgic, Combined effect of pores concavity and aspect ratio on the elastic properties of a porous material, International Journal of Solids and Structures 134 (2018) 161 – 172.

[12] I. Sevostianov, F. Chen, A. Giraud, D. Grgic, Compliance and resistivity contribution tensors of axisymmetric concave pores, International Journal of Engineering Science 101 (2016) 14 – 28.

[13] K. Kalo, D. Grgic, C. Auvray, A. Giraud, B. Drach, I. Sevostianov, Effective elastic moduli of a heterogeneous oolitic rock containing 3-d irregularly shaped pores, International Journal of Rock Mechanics and Mining Sciences 98 (2017) 20 – 32.

[14] S. A. Lurie, Y. Solyaev, L. N. Rabinskiy, P. O. Polyakov, I. Sevostianov, Mechanical behavior of porous $Si_3N_4$ ceramics manufactured with 3-D printing technology, Journal of Materials Science 53 (2018) 4796–4805.

[15] I. Sevostianov, V. Levin, M. Kachanov, On the modeling and design of piezocomposites with prescribed properties, Archive of Applied Mechanics 71 (11) (2001) 733–747.

[16] I. Sevostianov, N. Yilmaz, V. I. Kushch, V. Levin, Effective elastic properties of the particulate composite with transversely isotropic phases, International Journal of Solids and Structures 42 (2005) 455–476.

[17] V. M. Levin, M. G. Markov, Elastic properties of inhomogeneous transversely isotropic rocks, International Journal of Solids and Structures 42 (2005) 393–408.

[18] A. Giraud, Q. V. Huynh, D. Hoxha, D. Kondo, Effective poroelastic properties of transversely isotropic rocks-like composites with arbitrarily oriented ellipsoidal inclusions, Mechanics of Materials 39 (11) (2007) 1006–1024.

[19] P. Cosenza, D. Prêt, A. Giraud, S. Hedan, Effect of the local clay distribution on the effective elastic properties of shales, Mechanics of Materials 84 (2015) 55 – 74.

[20] K. Vasylevskyi, B. Drach, I. Tsukrov, On micromechanical modeling of orthotropic solids with parallel cracks, International Journal of Solids and Structures 144-145 (2018) 46 – 58.

[21] S. Seyedkavoosi, E. Vilchevskaya, I. Sevostianov, Randomly oriented cracks in a transversely isotropic material, International Journal of Solids and Structures 150 (2018) 222 – 229.

[22] F. Guerrero, I. Sevostianov, A. Giraud, On a possible approximation of changes in elastic properties of a transversely isotropic material due to an arbitrarily oriented crack, International Journal of Fracture 153 (2008) 169–176.

[23] S. Seyedkavoosi, I. Sevostianov, Modeling of the overall elastic behavior of a transversely isotropic material reinforced with arbitrarily oriented transversely isotropic platelets, Mechanics of Materials 132 (2019) 77 – 85.

[24] K. Du, L. Cheng, J. Barthélémy, I. Sevostianov, A. Giraud, A. Adessina, Numerical computation of compliance contribution tensor of a concave pore embedded in a transversely isotropic matrix, International Journal of Engineering Science 152 (2020) 103306.

[25] A. Trofimov, A. Markov, S. Abaimov, I. Akhatov, I. Sevostianov, Overall elastic properties of a material containing inhomogeneities of concave shape, International Journal of Engineering Science 132 (2018) 30 – 44.

[26] M. Kachanov, I. Sevostianov, Micromechanics of materials, with applications, no. 249 in Solid Mechanics and Its Applications, Springer, 2018.

[27] R. Hill, A self-consistent mechanics of composite materials, Journal of the Mechanics and Physics of Solids 13 (4) (1965) 213 – 222.

[28] J.-F. Barthélémy, Simplified approach to the derivation of the relationship between Hill polarization tensors of transformed problems and applications, International Journal of Engineering Science 154 (2020) 103326.

[29] M. Trott, The Mathematica Guidebook for Numerics, Springer, New York, 2006.

[30] T. Mori, K. Tanaka, Average stress in matrix and average elastic energy of materials with misfitting inclusions, Acta Metall. 21 (1973) 571–574.

[31] Y. Benveniste, A new approach to the application of Mori-Tanaka's theory in composite materials, Mechanics of Materials 6 (2) (1987) 147 – 157.

[32] A. Giraud, D. Hoxha, Q. V. Huynh, D. P. Do, V. Magnenet, Effective porothermoelastic properties of transversely isotropic rock-like composites, International Journal of Engineering Science 46 (2008) 527–550.
[33] I. Sevostianov, On the shape of effective inclusion in the Maxwell homogenization scheme for anisotropic elastic composites, Mechanics of Materials 75 (0) (2014) 45 – 59.
[34] A. Giraud, I. Sevostianov, V. Kushch, P. Cosenza, D. Prêt, J. Barthélémy, A. Trofimov, Effective electrical conductivity of transversely isotropic rocks with arbitrarily oriented ellipsoidal inclusions, Mechanics of Materials 133 (2019) 174 – 192.
[35] L. J. Walpole, Fourth-rank tensors in the thirty-two crystal classes: multiplication tables, Proceeding Royal Society London A391 (1984) 149–179.
[36] M. Hori, S. Nemat-Nasser, Overall moduli of solids with microcracks: Load induced anisotropy, Journal of the Mechanics and Physics of Solids 31 (2) (1983) 155–171.
[37] I. Sevostianov, M. Kachanov, Explicit cross-property correlations for anisotropic two-phase composite materials, Journal of the Mechanics and Physics of Solids 50 (2002) 253–282.
[38] I. Sevostianov, V. Levin, E. Radi, Effective viscoelastic properties of short-fiber reinforced composites, International Journal of Engineering Science 100 (2016) 61 – 73.
[39] A. Markov, A. Trofimov, S. Abaimov, I. Akhatov, On the applicability of replacement relations to tetrahedron-like inhomogeneities, International Journal of Solids and Structures 167 (2019) 1 – 13.